Development ePress. Posted online 5 March 2015
 | Development (2015) 142, 1-10 doi:10.1242/dev.115493

RESEARCH ARTICLE

Morphogenesis of the mouse neural plate depends on distinct roles of cofilin 1 in apical and basal epithelial domains

Joaquim Grego-Bessa[1], Jeffrey Hildebrand[2] and Kathryn V. Anderson[1,*]

ABSTRACT

The genetic control of mammalian epithelial polarity and dynamics can be studied *in vivo* at cellular resolution during morphogenesis of the mouse neural tube. The mouse neural plate is a simple epithelium that is transformed into a columnar pseudostratified tube over the course of ~24 h. Apical F-actin is known to be important for neural tube closure, but the precise roles of actin dynamics in the neural epithelium are not known. To determine how the organization of the neural epithelium and neural tube closure are affected when actin dynamics are blocked, we examined the cellular basis of the neural tube closure defect in mouse mutants that lack the actin-severing protein cofilin 1 (CFL1). Although apical localization of the adherens junctions, the Par complex, the Crumbs complex and SHROOM3 is normal in the mutants, CFL1 has at least two distinct functions in the apical and basal domains of the neural plate. Apically, in the absence of CFL1 myosin light chain does not become phosphorylated, indicating that CFL1 is required for the activation of apical actomyosin required for neural tube closure. On the basal side of the neural plate, loss of CFL1 has the opposite effect on myosin: excess F-actin and myosin accumulate and the ectopic myosin light chain is phosphorylated. The basal accumulation of F-actin is associated with the assembly of ectopic basal tight junctions and focal disruptions of the basement membrane, which eventually lead to a breakdown of epithelial organization.

KEY WORDS: SHROOM3, Actin, Cofilin, Epithelial polarity, Mouse genetics, Neural tube

INTRODUCTION

Animal development depends on the formation of stable epithelia that undergo regulated changes in cell shape and cell packing during morphogenesis. The regulation of epithelial organization and dynamics has been extensively studied in *Drosophila* and in mammalian epithelial cell lines; these studies have shown that a set of apical protein complexes that includes the Par complex, Crumbs complex, adherens junctions and tight junctions is required for the formation and maintenance of continuous epithelial sheets and for the distinct morphologies of different epithelia (Tepass, 2012; Roignot et al., 2013). Complex epithelial behaviors, including planar cell polarity (PCP), collective cell migration and branching morphogenesis, build upon this framework. In addition to the essential roles of epithelial organization in normal development, its disruption is a key step in carcinoma formation, invasion and metastasis (del Barrio and Nieto, 2002; Thiery et al., 2009).

[1]Developmental Biology Program, Sloan Kettering Institute, Memorial Sloan Kettering Cancer Center, 1275 York Avenue, New York, NY 10065, USA. [2]Department of Biological Sciences, University of Pittsburgh, Pittsburgh, PA 15260, USA.

*Author for correspondence (k-anderson@ski.mskcc.org)

Received 16 July 2014; Accepted 2 February 2015

Formation of the mouse neural tube provides an ideal context for genetic dissection of the regulation of morphogenesis, maintenance and dynamics of a complex mammalian epithelium *in vivo*. The CNS of amniotes develops from a simple epithelium that undergoes a defined sequence of morphogenetic events during development (Schoenwolf, 1985; Colas and Schoenwolf, 2001). The early neural plate of the mouse embryo arises from the dorsal ectoderm in a simple, single-layered epithelium. As neural progenitors proliferate, the neural plate thickens as cells elongate along their apicobasal axis and become tightly packed, while retaining their links to both the apical surface and the basement membrane of the epithelium. As the cells pack, their nuclei become stacked, creating a pseudostratified epithelium (Eom et al., 2013). At the same stage, neural tube closure initiates with the formation of a midline hinge-point in cells that will form the floor plate of the neural tube. Through highly orchestrated cell shape changes, including apical constriction, the neural plate folds and the dorsalmost cells join to create a closed tube. Understanding the mechanisms of neural tube closure is important for human health, as neural tube defects are among the most common human congenital malformations, affecting 0.5-2/1000 established pregnancies worldwide (Mitchell, 2005).

Genetic screens and targeted mutations have identified more than 100 genes that are required for mouse neural tube closure, regulating processes as diverse as patterning, PCP and organization of the actin cytoskeleton (Copp and Greene, 2010). Mutations in a number of genes that affect F-actin organization cause failure of closure of the cranial neural tube, including *Shroom3* mutants, double mutants in the *Abl Arg* (*Abl1 Abl2*) genes, double mutants in *Mena* (*Enah*) and profilin genes, and *Mena Vasp* double mutants (Hildebrand and Soriano, 1999; Koleske et al., 1998; Lanier et al., 1999; Menzies et al., 2004). Mutations in the gene encoding the actin regulator CFL1 also cause a completely penetrant failure of cranial neural tube closure (Gurniak et al., 2005).

Members of the cofilin family of proteins coat F-actin filaments, which can cause F-actin severing and depolymerization and promote the recycling of monomeric actin to allow dynamic reorganization of the actin cytoskeleton (Bamburg et al., 1999; Bernstein and Bamburg, 2010). Biochemical and cell-based studies have defined a central role for cofilin in the formation of lamellipodia and invadopodia in migrating and invading cells (Bravo-Cordero et al., 2013). Increased activity of cofilin is observed in invasive tumors and this is believed to make an important contribution to metastasis (Wang et al., 2007).

Genetic studies have revealed that cofilin has a variety of cellular functions *in vivo*, in addition to its roles in cell migration. It is required for cytokinesis *in vivo* in yeast, *Drosophila* and *C. elegans* (Gunsalus et al., 1995; Ono et al., 2003; Mendes Pinto et al., 2012). Cofilin is also important in epithelial cells: it is required for the organization of the *Drosophila* retinal epithelium (Pham et al., 2008) and plays a role in PCP in *Drosophila* and in mouse (Blair et al., 2006; Zhang et al., 2011; Mahaffey et al., 2013). Of the three

Development (2015) 142, 1-10 doi:10.1242/dev.115493

mammalian cofilin genes, only cofilin 1 (*Cfl1*) is essential for embryonic development. Homozygous *Cfl1* null embryos die at mid-gestation [approximately embryonic day (E) 10.0] with an open cranial neural tube (Gurniak et al., 2005). Sequence changes in human *CFL1* have also been associated with an increased risk of spina bifida (Zhu et al., 2007), suggesting that cofilin has a conserved role in neural epithelial organization.

Here we define the cofilin 1-dependent cellular mechanisms that regulate neural tube closure in mice. Cofilin is enriched in both the apical and basal domains of the wild-type neural plate and *Cfl1* mutants have dramatic and distinct defects in these two domains. F-actin is localized apically in the wild-type neural plate, but is enriched in both apical and basal domains in the *Cfl1* mutant neural plate. Despite the defects in the organization of F-actin, we find that apical polarity complexes, including adherens junctions, the Par and Crumbs complexes, as well as Shroom3, are correctly localized in the *Cfl1* mutant neural plate. However, phosphorylation of apical myosin II regulatory light chain (MLC2; MYL9), which is coupled to activation of actomyosin, is blocked in *Cfl1* mutants, indicating that cofilin 1 is required for the apical activation of actomyosin that is necessary for neural tube closure. By contrast, activated actomyosin accumulates in the basal domain in *Cfl1* mutants. Because cofilin 1 has opposing effects on actomyosin in the apical and basal domains of the neural epithelium, we suggest that apically localized proteins switch cofilin from a basal inhibitor of actomyosin to an apical activator of actomyosin contractility. Shortly after the basal accumulation of F-actin is detected, tight junction-like structures form on the basal side of the neural plate, and this is followed by focal disruptions of the basement membrane that lead to a disruption of epithelial organization that is reminiscent of the breakdown in epithelial organization associated with tumor progression.

RESULTS

Loss of apically and basally enriched cofilin 1 prevents neural tube closure

Embryos homozygous for a null allele of *Cfl1* fail to close the cranial neural tube (Gurniak et al., 2005). We identified an ENU-induced allele of *Cfl1* [$Cfl1^{C5}$ (García-García et al., 2005)] in which a T-to-A transversion in the coding sequence produces an F101I amino acid substitution adjacent to the actin-binding domain, producing a phenotype similar to that of the null allele (Mahaffey et al., 2013). The $Cfl1^{C5}$ neural tube had the normal sharp bend at the floor plate, but was open as far caudal as the heart, where the most dorsal neural plate curved away from the midline (Fig. 1Aii). The morphology of the $Cfl1^{C5}$ neural tube was also abnormal at more caudal positions, where it was closed (Fig. 1Aiii). The open neural tube was not associated with abnormal patterning of cell types in the developing brain (supplementary material Fig. S1) and instead appears to be due to defective morphogenesis.

Immunostaining of sections of the wild-type (WT) E9.5 neural plate showed that CFL1 protein was enriched at both the apical and basal edges of the epithelium (Fig. 1B,C). Almost no staining was detected in $Cfl1^{tm1Wit}$ null embryos (supplementary material Fig. S2A-D) and CFL1 staining was reduced in $Cfl1^{C5}$ neural tube (supplementary material Fig. S2G,H), consistent with reduced levels of CFL1 in $Cfl1^{C5}$ mutant embryos (Mahaffey et al., 2013). Apical CFL1 overlapped with the position of the adherens junctions and the apical F-actin belt, and was also present in apical caps, as visualized both in transverse sections (Fig. 1B; supplementary material Fig. S2E,F) and by en face imaging (supplementary material Fig. S2I).

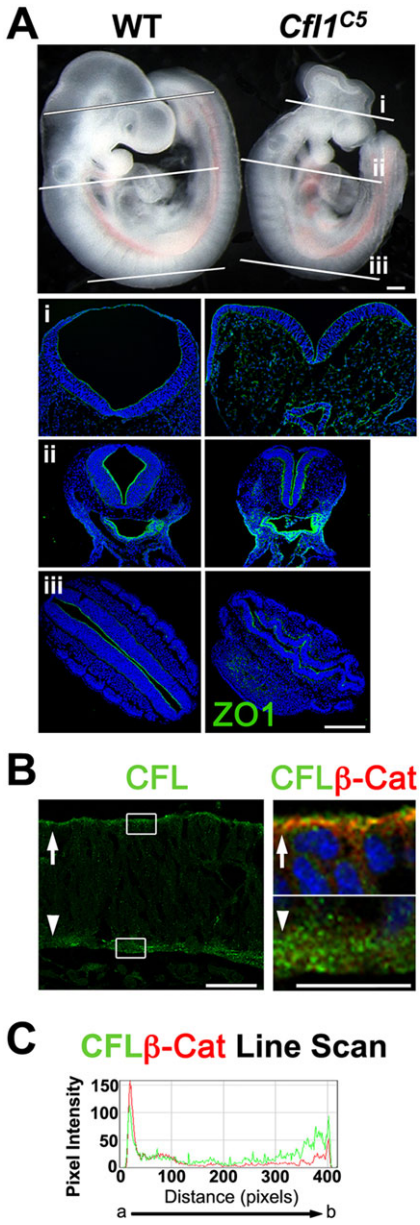

Fig. 1. Apically and basally enriched cofilin 1 is required for neural tube closure. (A) Wild-type (WT) and homozygous $Cfl1^{C5}$ E9.5 mouse embryos. Transverse sections are at cephalic (i) and branchial arch (ii) levels and longitudinal sections are along the caudal neural tube (iii). ZO1 is green. (B) Cofilin/ADF and β-catenin expression in the E9.5 WT cephalic neural plate; apical is up. Insets are apical and basal details at 4× original magnification. Arrows point to apical, arrowheads point to basal. (C) Pixel intensity quantification along a representative apicobasal trace of 20 pixels width of CFL1 (green) and β-catenin (red) double immunofluorescence in transverse sections of the E9.5 WT neural plate. a, apical; b, basal. Blue is DAPI. Scale bars: 200 µm in A; 30 µm in B; 15 µm in insets in B.

CFL1 is required for normal cell shape and cell number in the cephalic neural epithelium

Closure of the cranial neural tube in the WT mouse embryo depends on a sequence of cell shape changes that takes place in the neural plate between E8.0 and E9.5. Morphometric analysis of E9.5 neural epithelium showed that $Cfl1^{C5}$ neural plate was ~30% thinner than that of WT; as each cell extends from the base to the surface of the neural plate, individual cells were also ~30% shorter (apical to basal) (Fig. 2A,B). The apical surface area of $Cfl1^{C5}$ cells was more

Development (2015) 142, 1-10 doi:10.1242/dev.115493

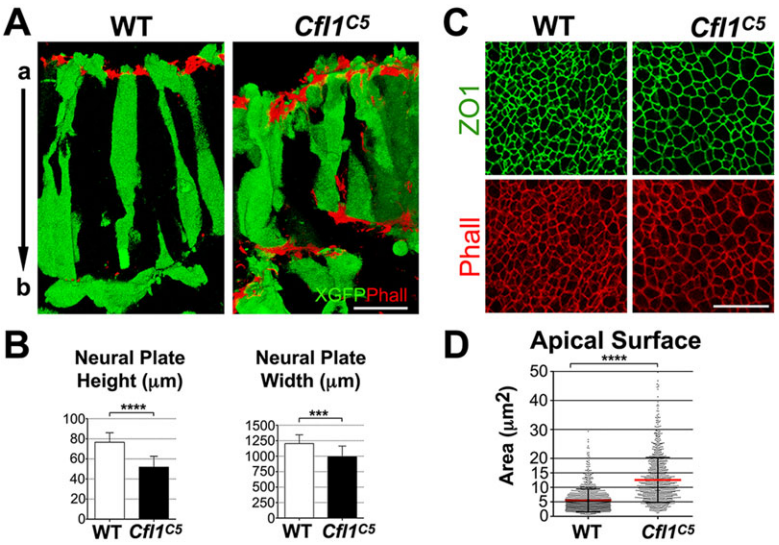

Fig. 2. Abnormal cell shape and distribution in the *Cfl1*^{C5} neural plate. (A) 3D reconstruction of cephalic neural plate (anterior to the first branchial arch), showing the thinner neural epithelium in *Cfl1*^{C5} and the apicobasal orientation of X-linked GFP^{+} neuroepithelial cells. Red is phalloidin (F-actin). (B) Quantification of neural plate height and width. Measurements are average±s.d. Height: WT, 77±10 μm; *Cfl1*^{C5}, 52±11 μm; ****P<0.0001, n=3 embryos. Width: WT, 1204±141 μm; *Cfl1*^{C5}, 988±175 μm; ***P=0.0004, n=3 embryos. (C) En face images of WT and *Cfl1*^{C5} E9.5 cephalic neural plate at a mediolateral position. ZO1 is green and F-actin is red. (D) Quantification of apical surface of cephalic neural plate cells. WT, 5.5±4.0 μm^2; *Cfl1*^{C5}, 12.5±8.0 μm^2; ****P<0.0001, n=3 embryos. Statistical analysis was performed using Student's t-test. Error bars indicate s.d. Scale bars: 20 μm.

than twice as large as in WT (Fig. 2C,D), so that the average volume of single cells was the same in WT and mutant (WT, 754±20 μm^3; *Cfl1*^{C5}, 830±41 μm^3; mean±s.d.; P=0.12; see Materials and Methods). Thus, CFL1 is required for the reduction in apical surface area that accompanies neural tube closure.

Despite the increased surface area of individual cells, the overall width of the *Cfl1*^{C5} neural plate was less than that of WT (Fig. 2B). Cell counts of transverse cephalic sections (from optic vesicle to the first branchial arch) showed that there were only 55% as many cells in the mutant neural plate as in WT (WT, 492±77 cells across the neural plate; *Cfl1*^{C5}, 274±78 cells; n=6 embryos each genotype; mean±s.d.). It has been shown that mutations in cofilin can slow cytokinesis (Chen and Pollard, 2011; Mendes Pinto et al., 2012). Based on BrdU incorporation, we found that the proliferative index was the same in WT and mutants (supplementary material Fig. S3A,B), but the mitotic index [phospho-histone H3 (PHH3)$^{+}$/total cells] increased from ∼11% in WT to ∼15% in the mutants (supplementary material Fig. S3C,D). Cyclin D1, which is expressed during G1 and G2 phases, was also upregulated ∼3-fold (supplementary material Fig. S3E). Thus, the duration of the cell cycle increased in the absence of CFL1.

In pseudostratified epithelia, nuclear position changes during the cell cycle in a process called interkinetic nuclear migration (INM), in which nuclei oscillate between a basal location during S phase and an apical position during mitosis (Spear and Erickson, 2012). In the WT neuroepithelium, ∼90% of the nuclei of PHH3^{+} cells (273/302) were localized apically, whereas only ∼3% of BrdU^{+} nuclei (48/1747) were apical. By contrast, only ∼75% of the nuclei of PHH3^{+} cells (242/318) were apically located in *Cfl1*^{C5} neural plate, and ∼8% of BrdU^{+} nuclei (123/1569) were apical (supplementary material Fig. S3A,C,F,G). Thus, INM is perturbed in the absence of CFL1. This is consistent with previous reports of the role of F-actin dynamics in INM (Norden et al., 2009) and might contribute to the slowed pace of cell cycle progression in the *Cfl1*^{C5} neural plate.

CFL1 prevents ectopic accumulation of F-actin

Cellular actin is present in both monomeric (globular, G-actin) and filamentous (F-actin) forms. The ratio of total F-actin/G-actin was ∼4-fold higher in whole *Cfl1*^{C5} embryo lysates than in WT (Fig. 3A), consistent with the role of CFL1 in F-actin severing and depolymerization (Bamburg et al., 1999). Transverse sections showed an increase in apical F-actin, marked by Rhodamine-phalloidin, in the E9.5 *Cfl1*^{C5} neural plate (Fig. 3B). Quantification showed that the maximum peak intensity of the apical F-actin signal in the E9.5 *Cfl1*^{C5} cranial neural plate was comparable to that of WT, but the apical F-actin domain was ∼30% expanded (Fig. 3B; see Materials and Methods). In addition, F-actin was also present in patches at the basal edge of the *Cfl1*^{C5} neural plate. The intensity of the F-actin signal in these basal patches was ∼3-fold higher in the mutant than in WT, both at E8.5 (not shown) and at E9.5 (Fig. 3B), based on line scans traced orthogonally to neural plate in regions that included apical and basal F-actin (yellow traces in Fig. 3B). The amount of total basal F-actin increased with time, with ∼25% of *Cfl1*^{C5} neural epithelial cells showing basal F-actin at E8.5; by E9.5, ∼60% of the neural epithelium had detectable basal F-actin (Fig. 3C), whereas fewer than 5% of WT cells showed basal F-actin at each stage.

To define the distribution of F-actin in individual cells of the tightly packed neural epithelium, we examined F-actin localization in E9.5 embryos that carried an X-linked *GFP* transgene that expresses cytoplasmic GFP mosaically in ∼50% of the cells in female embryos (Hadjantonakis et al., 2001). 3D renderings of GFP^{+} cells showed that some individual cells had both apical and basal F-actin (Fig. 3D; supplementary material Figs S4, S5 and Movies 1, 2).

Most apical proteins localize correctly in the *Cfl1*^{C5} neural plate

Because apical F-actin is important in the establishment of apicobasal polarity in epithelia (Ivanov et al., 2004; Ivanov, 2008), we analyzed the localization of polarized proteins in E9.5 *Cfl1*^{C5} embryos. At E9.5, when *Cfl1*^{C5} embryos were exencephalic, most apical markers in the cranial neural epithelium were localized to their normal domain. Markers of adherens junctions (N-cadherin and β-catenin), the Par complex (PAR3 and aPKC) and the Crumbs complex [CRB1/2/3, PATJ (INADL) and PALS1 (MPP5)] were confined to their normal apical location in the E9.5 *Cfl1*^{C5} cranial neural plate (Fig. 4A-F; supplementary material Fig. S6A-H). Primary cilia and centrosomes were present apically, as expected (Fig. 4G,H), and the Golgi marker GM130 (GOLGA2) was confined to the apical third of the cell, as in WT (supplementary material Fig. S6I,J).

SHROOM3, a PDZ domain-containing actin-binding protein, is a key regulator of cranial neural tube closure (Hildebrand and Soriano, 1999; Hildebrand, 2005; Nishimura and Takeichi, 2008).

Development (2015) 142, 1-10 doi:10.1242/dev.115493

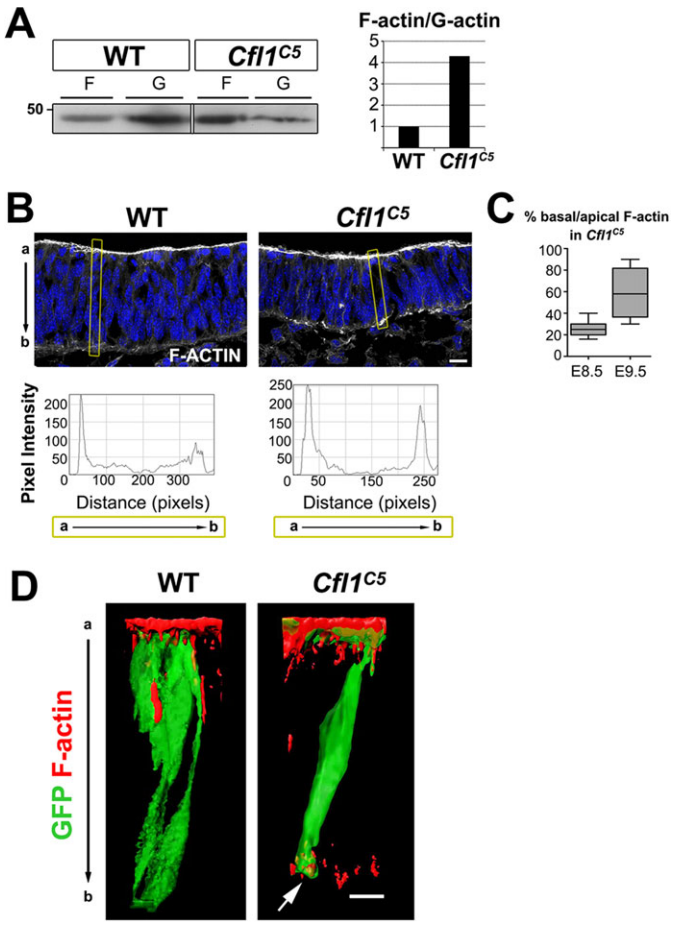

Fig. 3. F-actin accumulation in the *Cfl1*^{C5} neural plate. (A) Samples of supernatant (G-actin) and pellet (F-actin) were run in an SDS-PAGE gel and actin was quantitated by western blot. Values were normalized to WT set at 1.0. (B) Phalloidin-stained (white) transverse sections of the WT and *Cfl1*^{C5} E9.5 cephalic neural plate. Blue is DAPI. Plots beneath show pixel intensity quantification along an apicobasal trace of 20 pixels width (boxed in yellow) in E9.5 WT and mutant sections. The trace was orthogonal to the plane of the neural plate at a peak of ectopic basal fluorescence. (C) Box and whiskers plot showing the proportion of basal/apical F-actin (average Rhodamine-phalloidin fluorescence intensity) in mutant embryos at E8.5 and E9.5 in the cephalic neural plate. (D) 3D rendering of X-linked GFP expression (green) and phalloidin (red) of single E9.5 neural epithelial cells. Arrow indicates ectopic basal F-actin. Scale bars: 15 µm in B; 10 µm in D.

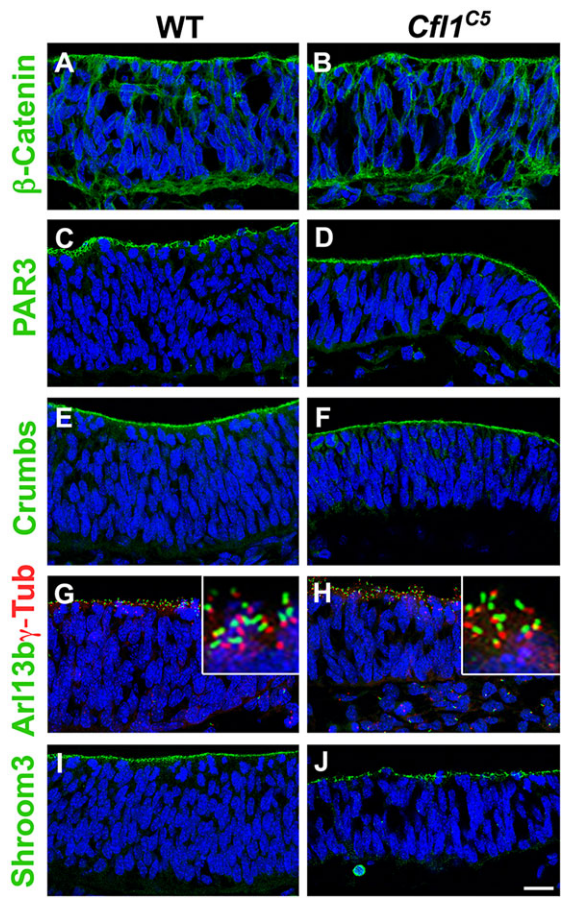

Fig. 4. Normal localization of apical markers in *Cfl1*^{C5} embryos. *z*-stack projections of three optical sections (total of 3 µm) from transverse sections of the cephalic neural plate of E9.5 WT and *Cfl1*^{C5} embryos stained for (A,B) β-catenin, (C,D) PAR3, (E,F) Crumbs (CRB1/2/3), (G,H) ARL13B (a membrane marker specifically expressed in cilia; green) and γ-tubulin (red) and (I,J) SHROOM3. Insets (G,H) are 8× original magnification of the apical domain. Blue is DAPI. Scale bar: 30 µm.

As in WT, SHROOM3 was localized to the apical domain of the *Cfl1*^{C5} neural plate (Fig. 4I,J) and the total amount of SHROOM3 in *Cfl1*^{C5} embryos was comparable to that in WT as assessed by western blot (Fig. 5E). Collectively, these results indicate that the apical cellular domain is established correctly in *Cfl1*^{C5} mutants.

CFL1 is required for the localization and activation of cytoplasmic actomyosin in the neural plate

In contrast to the apical polarity markers, a specific set of other polarized proteins became ectopically localized in a defined sequence in the *Cfl1*^{C5} neural plate between E8.0 and E9.5, the normal time of cranial neural folding and closure. F-actin was the first protein to appear ectopically on the basal side of the neural epithelium. Puncta of ectopic F-actin were detectable at E8.0 (Fig. 5B and see Fig. 7A).

Myosin-dependent apical constriction of cells of the neural plate is essential for neural tube closure (Hildebrand and Soriano, 1999; Hildebrand, 2005; Lee et al., 1983). At E9.5, non-muscle myosin heavy chain IIB (MHCIIB; MYH10) was present in its normal location near the apical surface of the neural plate in *Cfl1*^{C5} embryos, although the amount of apical MHCIIB was ~30% less than in WT (Fig. 5A). In addition, MHCIIB was highly enriched at the basal cortex of mutant epithelial cells (Fig. 5A). Line scan analysis showed that at some positions there was 2- to 3-fold more MHCIIB on the basal side of the *Cfl1*^{C5} neural plate than in WT, whereas MHCIIB was barely detectable at other basal positions (Fig. 5A). Western blot analysis of extracts from E9.5 embryo heads showed that the total level of MHCIIB was similar in WT and mutants (Fig. 5E), suggesting that MHCIIB was redistributed from the apical to the basal domain in the mutant neural epithelium.

Phosphorylation of MLC on Ser19 is a hallmark of actomyosin contractility (Bresnick, 1999). Like MHCIIB, phosphorylated MLC (pMLC) was highly enriched in the apical domain of WT neural epithelial cells, where it overlapped with F-actin at E8.0, E8.5 and E9.5 (Fig. 5B-D). At E8.0, when neural plate folding begins, the level of pMLC was greatly reduced in the apical *Cfl1*^{C5} neural plate. At the same developmental stage, pMLC was present ectopically on the basal side of the *Cfl1*^{C5} neural plate, where it overlapped with the ectopic F-actin (Fig. 5B). At E8.5 and E9.5, pMLC became further enriched basally, whereas it was barely detectable on the apical side of the mutant neural plate (Fig. 5C,D). Western blot analysis showed that, although the total amount of MLC was similar in WT and

Development (2015) 142, 1-10 doi:10.1242/dev.115493

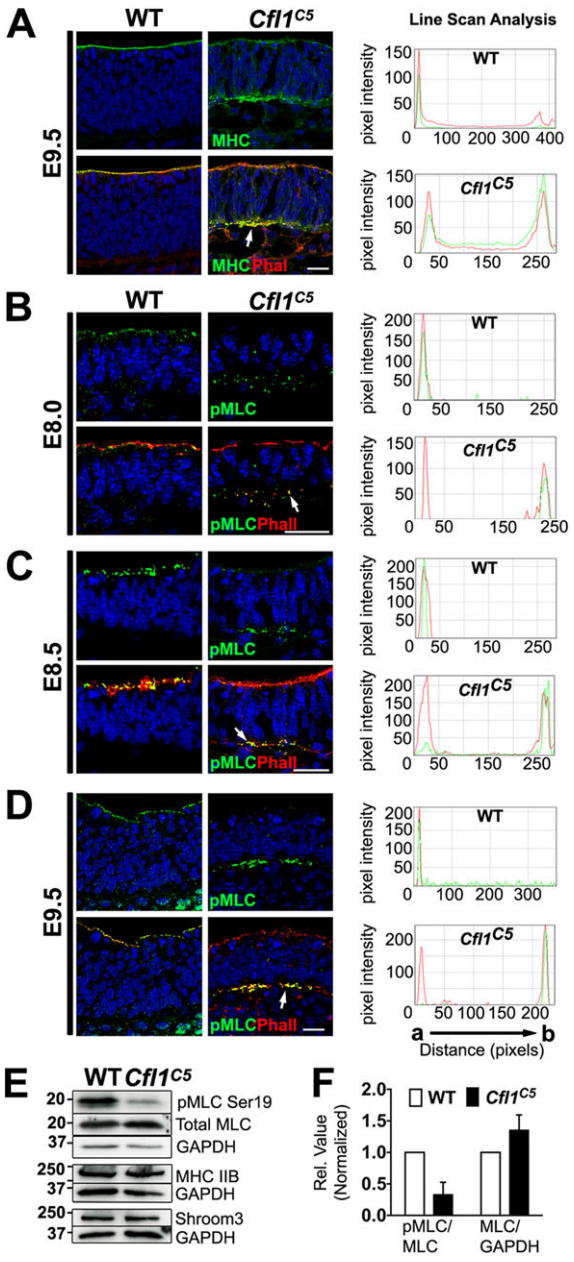

Fig. 5. Altered actomyosin in the *Cfl1*^{C5} neural plate. Single optical sections from transverse sections of the cephalic neural plate from WT and *Cfl1*^{C5} embryos showing expression of (A) MHC (MHC II-B) and F-actin at E9.5, (B) pMLC and F-actin at E8.0, (C) E8.5 and (D) E9.5; apical is up, basal is down. Arrows indicate overlap with ectopic F-actin. Blue is DAPI. Graphs show pixel intensity quantification along representative apicobasal traces 20 pixels wide in WT and mutant sections. (E) Western blot of MHCIIB, pMLC, total MLC, SHROOM3 and the respective GAPDH loading controls. A representative experiment out of three independent experiments is shown. Numbers indicate kDa. (F) Quantification of pMLC western blots from three independent experiments. Normalized *Cfl1*^{C5} values (WT set at 1): pMLC/MLC, 0.33±0.2; MLC/GAPDH, 1.35±0.24; Error bars indicate s.d. $P<0.05$ (Student's *t*-test). Scale bars: 20 µm.

mutant, there was only one-third as much pMLC in the mutant (Fig. 5E,F). The results suggest that there is a strong reduction of active actomyosin on the apical side of the *Cfl1*^{C5} neural plate.

Although the neural tube closure phenotype of *Shroom3* mutants is similar to that of *Cfl1* mutants and both proteins are required for apical actomyosin localization, the molecular phenotypes are distinct. It was previously reported that apical MHCIIB is reduced by half to two-thirds in *Shroom3* mutants (Hildebrand, 2005); we confirmed that observation and found that the amount of apical MHCIIB was reduced to a similar extent in *Shroom3* mutants as in the *Cfl1*^{C5} neural plate (Fig. 5A and Fig. 6A). However, apical F-actin was slightly reduced in the *Shroom3* mutant (Fig. 6B), whereas it was elevated in *Cfl1*^{C5}. Most strikingly, whereas the amount of apical pMLC was reduced in *Shroom3* mutants (Fig. 6C) it was undetectable in the *Cfl1*^{C5} neural plate, indicating that loss of CFL1 disrupts apical actomyosin contractility more profoundly than does the absence of SHROOM3. The effect of SHROOM3 was restricted to the apical domain, as no enrichment of basal MHCIIB or pMLC was detected in *Shroom3* mutants (Fig. 6A,C) and the basal pMLC in the *Cfl1*^{C5} neural plate did not overlap with SHROOM3 (supplementary material Fig. S7).

Tight junction proteins and pERM become basally localized in the *Cfl1*^{C5} neural plate

The tight junction proteins ZO1 and ZO2 (TJP1 and TJP2) were present in their normal apical location in *Cfl1*^{C5} neural plate, consistent with the normal location of other apical markers (Fig. 7); again, this differed from the *Shroom3* phenotype, where the level of apical ZO1 was decreased (Fig. 6D). However, ectopic ZO1 accumulated on the basal side of the E8.5 *Cfl1*^{C5} neural plate in puncta that colocalized precisely with the basal puncta of F-actin (Fig. 7A,B). By E9.5, there were patches of cells that showed continuous basal expression of both ZO1 and ZO2 (Fig. 7C). By contrast, loss of SHROOM3 did not lead to ectopic basal ZO1 (Fig. 6D). Transmission electron microscopy (TEM) of the E9.5 *Cfl1*^{C5} neural plate showed electron-dense material both at apical junctions (supplementary material Fig. S8A,B) and at the closely apposed membrane of adjacent cells near the basal surface of the mutant neural plate (in 2/2 mutant embryos; Fig. 7D; supplementary material Fig. S8D), suggesting that ectopic ZO1 and ZO2 assembled into basal tight junction-like structures in the absence of CFL1.

Phosphorylated (active) ERM (pERM) proteins, which can link the plasma membrane to F-actin (Ben-Aissa et al., 2012; Tsukita et al., 1994), localized normally to the apical cortex of the *Cfl1*^{C5} neural plate at E8.5. However, pERM was detected at the basal surface of the mutant neural plate at E9.5 (Fig. 7A-C). Because pERM became ectopically localized only after the time when the neural tube should be closed, it is likely that the basal localization of pERM is a consequence of the morphological disruption of the mutant neural plate rather than a cause of the neural tube closure defect.

The basement membrane becomes disrupted in the *Cfl1* mutant neural plate

In addition to the ectopic localization of myosin and tight junction proteins to the basal side of the *Cfl1*^{C5} neural epithelium, we observed a gradual disruption of the basement membrane of the mutant neural plate. Laminin is a constituent of the basement membrane beneath the neural epithelium. At E8.0, laminin expression appeared normal in the *Cfl1*^{C5} neural plate; however, there were irregular breaks in laminin at the position of ectopic F-actin as early as E8.5 and the organization of laminin became more abnormal by E9.5 (Fig. 8A). Expression of fibronectin, another basement membrane protein, was also discontinuous at E9.5 in the mutant (supplementary material Fig. S9). Abnormalities in the basement membrane of the *Cfl1*^{C5} neural plate were also apparent by TEM (Fig. 8B and Fig. 7D). In addition to the loss of basement membrane, ectopic laminin and fibronectin were detected in the middle of the neural plate (Fig. 8A; supplementary material Fig. S9).

Development (2015) 142, 1-10 doi:10.1242/dev.115493

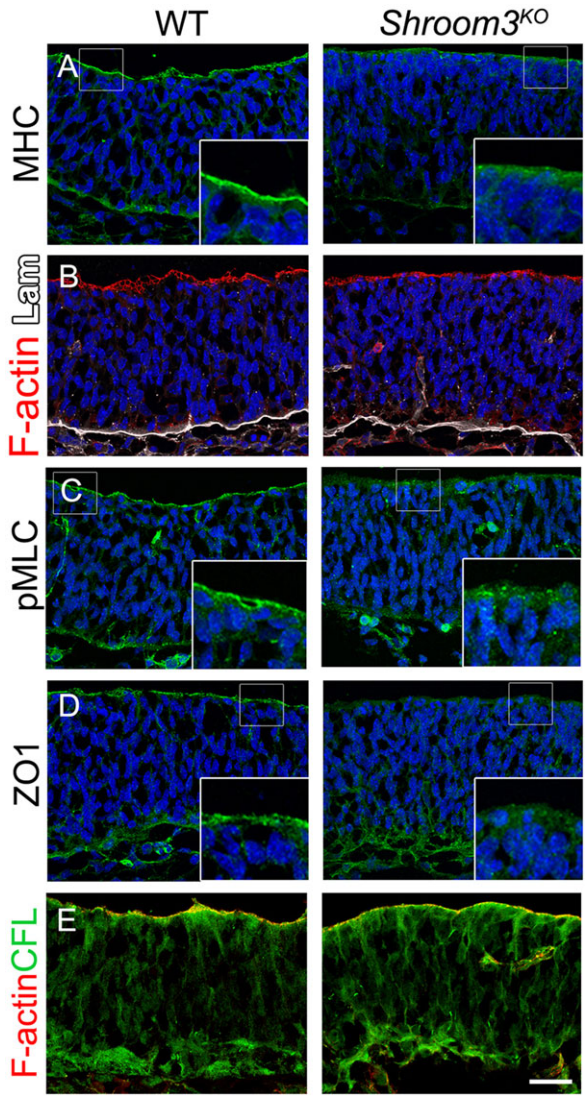

Fig. 6. Localization of apical markers in *Shroom3* mutant embryos. *z*-stack projection of three optical sections (total of 3 µm) from transverse sections of the cephalic neural plate of E9.5 WT and *Shroom3* mutant embryos stained for (A) MHC (MHC II-B), (B) F-actin (red) and laminin (white), (C) pMLC, (D) ZO1 and (E) cofilin (green) and F-actin (red). Blue is DAPI. Insets are 8× original magnification of the apical domain. Scale bar: 30 µm.

Scanning electron microscopy (SEM) images of the apical surface of E9.5 neural plate revealed the presence of cell clusters above the apical surface of the neural plate in every mutant embryo analyzed at E9.5; single embryos had a few to dozens of these structures (Fig. 8C). Transverse sections also showed that the E9.5 embryos analyzed had groups of cells that protruded from the apical side of the neural epithelium. No apical cell clusters were detected in transverse sections of E8.5 mutants, but by E9.5 apical protrusions occupied ~8 ±2% of the width of $Cfl1^{C5}$ cephalic neural plate (n=3; total of ten measurements). 3D projections of immunostained transverse sections revealed that these ectopic clusters contained cells that expressed both apical and basal markers, creating what appeared to be a multilayered epithelium (Fig. 8D). We also detected individual cells on the apical surface of the neuroepithelium in $Cfl1^{C5}$ embryos expressing X-linked GFP (Fig. 8E), suggesting that the apical extrusion of cells from the neural plate could be a property of individual cells rather than aberrant folding of the neural plate. At a lower frequency, we observed cells that escaped the basal aspect of the neural plate at the breaks in the basement membrane (~1 basal cell cluster in every seventh 10 µm transverse section) (Fig. 8F). Thus, CFL1 is required to maintain the integrity of the neural epithelium.

DISCUSSION

The analysis presented here defines a set of functions of CFL1-mediated actin dynamics in the organization of the neural epithelium. CFL1 is enriched in both the apical and basal domains of neural epithelial cells and it has different roles in the two domains. Consistent with the actin-severing and depolymerizing activities of cofilin, there is an increase in F-actin in the absence of CFL1 both apically and basally: there is an increase in F-actin apical to the adherens junctions and there are ectopic patches of F-actin at the base of the neural epithelium in *Cfl1* mutant embryos. A similar apical expansion and ectopic basal accumulation of F-actin was seen in clones in the ovarian follicular epithelium that lack *twinstar*, the single *Drosophila* homolog of cofilin (Baum and Perrimon, 2001). Even though loss of CFL1 causes increased F-actin in both domains, the data suggest that it has distinct functions that depend on the intracellular context: in the apical domain of the neural plate CFL1 is required for activation of cytoplasmic myosin, contraction of the apical actin ring and therefore for neural tube closure, whereas the basal activity of CFL1 prevents the basal formation of active actomyosin and tight junctions and helps maintain the basement membrane (Fig. 8G).

CFL1 is required for apical actomyosin localization and activity during neural tube closure

Although both cytoplasmic MHCIIB and MLC are present at normal levels in the *Cfl1* mutant neural plate, there is no detectable apical active pMLC in the absence of CFL1. While it is surprising that cofilin is required for the activation of actomyosin contraction, a precedent for a function of cofilin in promoting actomyosin activity comes from analysis of cytokinesis. During cytokinesis in fission yeast and *C. elegans*, the actin filaments in the contractile ring are highly dynamic and undergo rapid polymerization and depolymerization (Pelham and Chang, 2002; Zumdieck et al., 2007). Studies in budding yeast indicate that cofilin-mediated actin depolymerization drives actomyosin ring contraction during cytokinesis and suggested that the role of myosin is primarily to enhance actin depolymerization (Mendes Pinto et al., 2012). We propose that the apical ring constriction that drives neural tube closure is also driven by cofilin-mediated actin depolymerization and that activation of the apical myosin motor depends on this cofilin-mediated actin depolymerization.

The neural tube closure defect in *Cfl1* mutants is morphologically similar to that of *Shroom3* mutants and both mutants prevent normal apical constriction of neural plate cells, but their mechanisms of action are distinct. The ability of SHROOM3 to change cell shape depends on cytoplasmic myosin and on Rho kinase (ROCK) (Hildebrand, 2005), and SHROOM3 can recruit ROCK to adherens junctions (Nishimura and Takeichi, 2008). As in *Cfl1* embryos, there is a reduction of apical MHC II-B and pMLC in *Shroom3* mutants (Hildebrand and Soriano, 1999) (Fig. 6). However, there is an expansion in apical F-actin in the $Cfl1^{C5}$ neural plate, whereas apical F-actin is decreased in *Shroom3* mutants. The activity of SHROOM3 appears to be confined to the apical domain, whereas cofilin acts both apically and basally. As we do not see a reduction of apical SHROOM3 in the $Cfl1^{C5}$ neural plate, and cofilin is localized normally in *Shroom3* mutants (Fig. 6E), we suggest that CFL1 and SHROOM3 act in parallel to control contraction of the apical actomyosin ring.

Development (2015) 142, 1-10 doi:10.1242/dev.115493

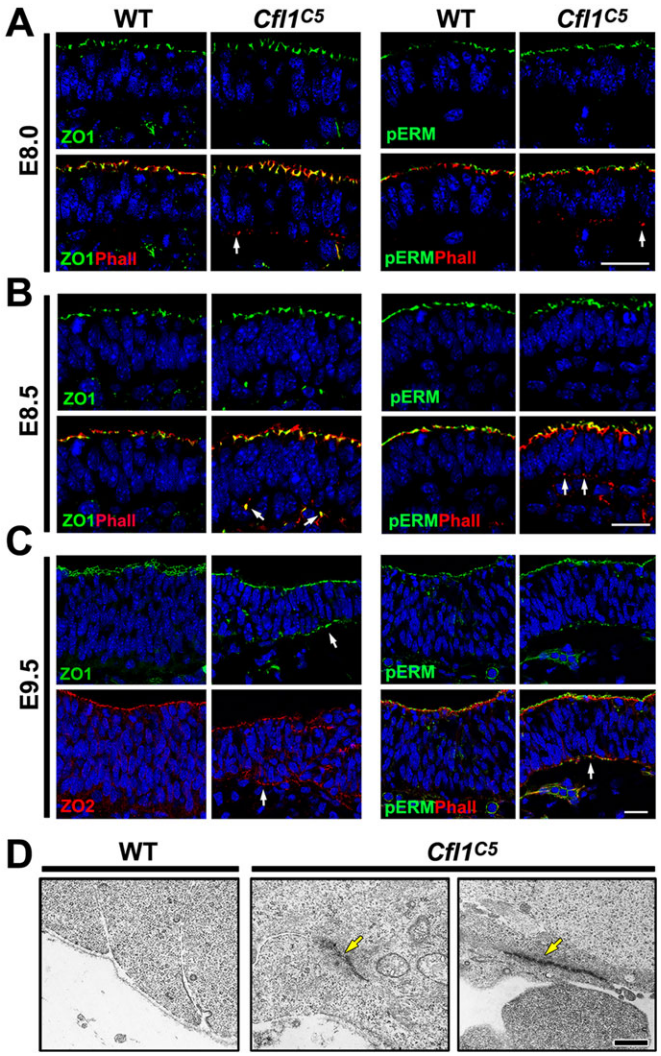

Fig. 7. Actin-associated proteins in the neural plate become progressively basally localized. (A,B) Transverse sections of the cephalic neural plate from WT and *Cfl1*^{C5} embryos showing the expression of F-actin, ZO1 and pERM in (A) E8.0 and (B) E8.5 embryos. (C) Expression of F-actin, ZO1, ZO2 and pERM in E9.5 embryos. Arrows (A-C) indicate ectopic localization or overlap with F-actin. Blue is DAPI. (D) Representative TEM images of the basal domain of E9.5 cephalic neural plate (*n*=2 embryos). Arrows indicate regions of ectopic electron-dense particles in two mutant embryos. Apical is up, basal is down. Scale bars: 20 µm in A-C; 1 µm in D.

CFL1 organizes the basal domain of the neural epithelium

While CFL1 is required for the apical activation of actomyosin, our data suggest that basal CFL1 has the opposite activity: it prevents the accumulation of basal cytoplasmic myosin and pMLC. Although the defects in apical myosin activation are sufficient to explain the neural tube defect in *Cfl1*^{C5} mutants, the activated basal actomyosin might also contribute to the defects in neural morphogenesis.

In the absence of CFL1 activity, myosin redistributes from the apical to the basal domain of the neural plate, raising the possibility that the basal accumulation of myosin could be a passive consequence of the loss of apical myosin. However, given that cofilin is localized basally and that basal F-actin accumulates prior to, or at the same time as, pMLC, it is likely that basally localized cofilin redirects myosin to the basal side of the neural plate. The lack of basal accumulation of cytoplasmic myosin in *Shroom3* mutants, in which apical MHCIIB is also decreased, supports the hypothesis that basal cofilin has a direct role in neural plate organization.

The inactivation of myosin by basally localized cofilin is similar to an activity of cofilin described recently in HeLa cells, in which cofilin competes with myosin for binding to F-actin and thereby inhibits the accumulation and activity of cortical actomyosin (Wiggan et al., 2012). We suggest that in the neural epithelium basal cofilin activity blocks actomyosin formation, as in HeLa cells and that, by contrast, apical cofilin promotes actomyosin activation, as in the contractile ring. We suggest that apically restricted protein(s), such as the Par complex or SHROOM3, act as a switch that determines the nature of the activity of apical cofilin (Fig. 8G).

One of the dramatic effects of the loss of *Cfl1* is the basal appearance of the tight junction proteins ZO1 and ZO2 and the assembly of basal structures that resemble tight junctions. This apparent tight junction-promoting effect of decreased cofilin activity is consistent with previous studies that showed that treatment of cells with jasplakinolide, a small molecule that prevents actin severing and mimics the effects of cofilin loss, accelerates the formation of apical tight junctions in culture (Ivanov et al., 2005).

Although ZO1 binds directly to F-actin (Fanning et al., 1998), it was nevertheless surprising that removal of cofilin was sufficient to promote the formation of basal tight junction-like structures. However, previous studies in cultured epithelial cells suggested a pathway by which active cofilin negatively regulates tight junction formation. Knockdown of PAR3 in MDCK cells disrupts the formation of tight junctions (Chen and Macara, 2005). In these cells, PAR3 inhibits the activity of LIMK2, which phosphorylates (and thereby inactivates) cofilin (Chen and Macara, 2006). This pathway is consistent with our findings and would suggest that CFL1 is required specifically in the WT basal domain, where PAR3 is not present, to prevent tight junction formation. However, mouse *Limk1/2* double mutants are viable and fertile (Meng et al., 2004), indicating that negative regulation of tight junction formation involves other, as yet unrecognized players that control the activity of CFL1.

Cofilin, epithelial integrity and tumorigenesis

We observed that after F-actin and tight junction proteins accumulate basally, the basement membrane becomes disrupted and this is associated with a global disruption of epithelial organization. The most common defect observed in epithelial organization is the apical extrusion of single cells or groups of cells from the apical surface. It has been suggested that loss of basement membrane contact, without an epithelial-to-mesenchymal transition, can lead to the apical extrusion of cells out of the epithelium and this can be an early event in cancer progression (McCaffrey and Macara, 2011). At a lower frequency, we also observed clusters of cells extruded from the basal aspect of the neural plate at the position of breaks in the basement membrane.

Many studies in cultured cells and tumors have indicated that upregulation of cofilin is associated with increased motility and metastasis (Wang et al., 2006, 2007). However, downregulation of cofilin has also been associated with tumorigenesis in MHCC97-H hepatocellular carcinoma (HCC) cells with high metastatic potential (Ding et al., 2004) and in ovarian surface epithelium (OSE) cells from *BRCA1* carriers (Smith-Beckerman et al., 2005). Mutations in *Cfl1* are rare in tumors, and both increased and decreased copy number have been seen in tumors (Sinha et al., 1999; Unwin et al., 2009). Our findings suggest that *Cfl1* has a complex role in tumor progression: although increased CFL1 activity may promote

Development (2015) 142, 1-10 doi:10.1242/dev.115493

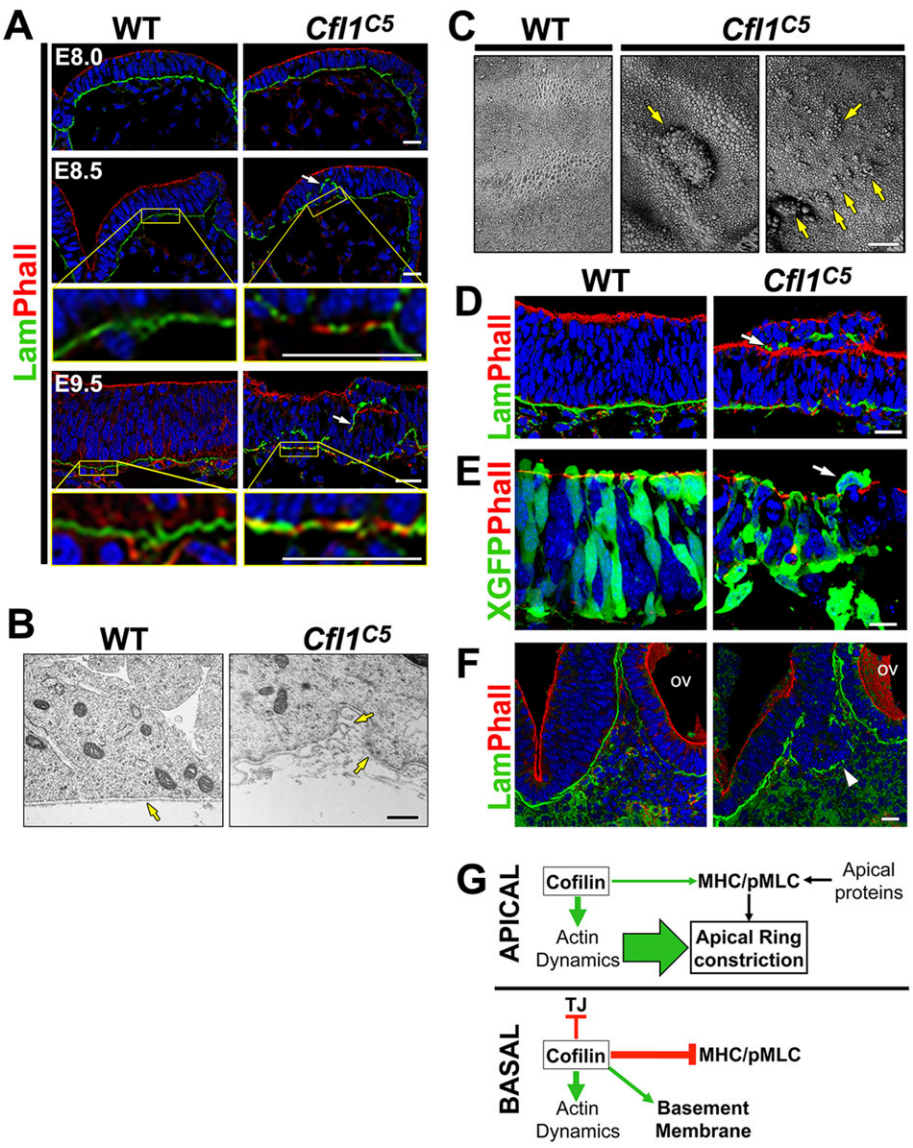

Fig. 8. Disruption of the basement membrane in the *Cfl1*^{C5} neural plate. (A) Time sequence of laminin (green) and F-actin (red) localization in transverse sections of the cephalic neural plate. Arrows indicate ectopic laminin expression in the mutant. The regions in the yellow boxes are shown at higher magnification beneath. (B) TEM of the basal domain of the E9.5 neural plate. Arrows indicate basement membrane. (C) SEM of the apical surface of E9.5 anterior neural plate. Arrows indicate cell clusters extruding from the apical surface of the mutant. (D) 3D reconstruction of a 12 µm transverse section of the E9.5 cephalic neural plate with an ectopic apical cell cluster in the mutant that expresses laminin and F-actin. Arrow points to ectopic laminin. (E) Single optical section of X-linked GFP^{+} cells and F-actin (red) expression in E9.5 cephalic neural plate. Arrow indicates a single cell above the apical surface of the neural plate. (F) Ectopic basal cell cluster (arrowhead) in a 3D reconstruction of a 25 µm transverse section of the E10 mutant neural plate. OV, otic vesicle. (G) Model of CFL1 activity during neural tube closure. Apical CFL1 is required for contraction of the apical actin ring and activation of cytoplasmic myosin. Basal CFL1 is required to prevent basal formation of active actomyosin and tight junctions (TJ) and for maintenance of the basement membrane. Apical proteins such as PAR3 or SHROOM3 might direct distinct consequences of CFL1 activity in the apical versus basal domain. Blue is DAPI. Scale bars: 30 µm in A,C,D,F; 1 µm in B; 15 µm in E.

metastasis, CFL1 also stabilizes epithelial integrity and therefore may help prevent invasion and metastasis.

MATERIALS AND METHODS

Mouse strains

C5 is a recessive ENU-induced mutation associated with a F101I missense substitution (Mahaffey et al., 2013). The *Cfl1*^{tm1Wit} null allele was a gift from Walter Witke (Rheinische Friedrich-Wilhelms University, Bonn, Germany). The X-linked *GFP* transgene was a gift from Anna-Katerina Hadjantonakis (Hadjantonakis et al., 2001). All the lines were backcrossed onto the FVB background for at least four generations.

Phenotype analysis

Embryos were dissected and processed for imaging following established protocols (Lee et al., 2007, 2010). SHROOM3 antibodies were from Jeffrey Hildebrand and from Masatoshi Takeichi (RIKEN Center for Developmental Biology, Kobe, Japan) and were used at 1:200 for immunostaining and 1:1000 for western blots. ARL13B antibody (Caspary et al., 2007) was used at 1:2000. The cofilin/ADF antibody was a gift from James R. Bamburg (Colorado State University, CO, USA) and was used at 1:500. The Crumbs antibody was a gift of B. Margolis (University of Michigan) and was used at 1:200. Commercial antibodies were as follows. Sigma: cofilin (C-8736), fibronectin (F-3648), laminin (L-9393), γ-tubulin (T-6557), all 1:1000. BD Biosciences: aPKC (610208), 1:200; GM130 (610822), 1:400; ZO2 (611560), 1:200. Santa Cruz Biotechnology: N-cadherin (sc-7939), 1:200 for immunofluorescence (IF); GAPDH (sc-32233), 1:5000 for western blot (WB). Invitrogen: ZO1 (33-9100), 1:200 for IF. Millipore: PAR3 (07-330). Cell Signaling: pMLC2 (3671), 1:50 for IF and 1:1000 for WB; pERM (3141), 1:50; ZO2 (2847), 1:200. Upstate: phospho-histone H3 (06-570), 1:400. Hybridoma Bank and Covance: MHCIIB (CMII-23; PRB-445P), 1:50 and 1:200, respectively, for IF and 1:1000 for WB.

Rhodamine-phalloidin (Invitrogen) was used at 1:200. BrdU labeling was carried out as described (Bloomekatz et al., 2012). Immunofluorescence staining was performed with Alexa Fluor-conjugated secondary antibodies (Invitrogen) diluted 1:400. Sections were counterstained with DAPI to stain nuclei. Samples were mounted using Vectashield (Vector Labs) or ProLong Gold (Life Technologies) mounting media, and slides were imaged with SP5 and SP8 confocal microscopes (Leica) with a 63×0.5 NA lens, at a resolution of 1024×1024. Maximum intensity was set in the apical domain, and images with apical non-saturated signal on the neural plate were taken. Images shown are single optical sections unless stated otherwise. Images were analyzed using Volocity software (PerkinElmer). The immunofluorescence data presented in the figures are representative of images of at least three embryos.

Development (2015) 142, 1-10 doi:10.1242/dev.115493

Morphometric analysis

Transverse sections of three embryos [stage matched by the number of somites (21-24)] were stained with DAPI. Height (apical to basal) and width (from left to right, along the apical domain) of cephalic neural plate transverse sections between the optic vesicle and first branchial arch were quantified from the length of traced lines using ImageJ 10.2 (NIH). Total number of cells per transverse section of neural plate was obtained from the total number of nuclei (DAPI stained) in single optical transverse sections of the cephalic region in three different embryos. To calculate average cell volume, we assumed that cell shape is a rectangular solid, and calculated the total number of cells in a constant surface (2500 μm^2) of neural plate. We calculated the volume using as z=neural plate height; then we divided this volume by the average number of cells per section: WT=(2500 μm^2×77 μm)/number of cells; $Cfl1^{C5}$=(2500 μm^2×52 μm)/number of cells; P=0.12 (non significant) by Student's t-test; n=4 embryos, two measurements per embryo.

Fluorescence quantification and image processing

Pixel intensity along the apicobasal axis was determined on single optical sections taken from confocal images (Leica SP5) fluorescently labeled by staining with specific antibodies (RGB color) or phalloidin (grayscale). Plots of pixel intensity were made from lines 20 pixels wide traced with ImageJ.

To quantify the percentage of basal/apical F-actin, average fluorescence intensity was quantified along ten lines, of 20 pixels width each, from left to right (width) of the neural plate (n=3 embryos) using ImageJ. Images analyzed were z-stack projections of three confocal optical sections taken every 1 μm of the cephalic region.

The shift in the distribution of apical F-actin was analyzed by measuring pixel intensity of phalloidin staining in the apical domain of the neural plate in single optical sections along an apicobasal trace 20 pixels wide and 100 pixels long in both WT and mutant (n=3 embryos, five scans/embryo). To compare the F-actin distributions relative to the apical F-actin belt, we manually positioned the maximum intensity of F-actin (which corresponds to the F-actin belt) on pixel number 20 of the trace to compare and statistically analyze every position between WT and $Cfl1^{C5}$. The P-value for the difference in intensity was calculated for each pixel along the 100 pixels of the trace; the intensity was greater at each position from pixel number 7 to 26 (except pixels 19 and 20); $P \leq 0.05$, Student's t-test. From these data we generated a curve in which x=distance in pixels and y=pixel intensity; based on this analysis we compared the total intensity of apical phalloidin staining from pixel 7 to 26, which gave an area of 6109 arbitrary units (a.u.) in WT and 9058 a.u. in $Cfl1^{C5}$.

For the 3D reconstructions shown in Fig. 3C, images were taken from whole-mount female X-linked GFP-positive E9.5 embryos labeled with TRITC-phalloidin with a Leica SP8 confocal microscope using a 63×0.5 NA lens. IMARIS 7.6 software (Bitplane) was used for 3D rendering and reconstruction. For 3D reconstructions of embryo sections, images were taken from 12 or 40 μm thick sections using a Leica SP5 confocal microscope with a 63×0.5 NA lens. Volocity software was used to generate 3D reconstructions. Apical surface area quantification was determined from en face images taken with a Leica SP5 inverted confocal microscope and 63×0.5 NA lens, and analyzed by Volocity software.

Electron microscopy

E9.5 embryos were fixed with 2% paraformaldehyde and 2.5% glutaraldehyde in 0.1 M sodium cacodylate buffer. For SEM, embryos were dissected to expose the lumen of the cephalic neural tube in 0.1 M cacodylate buffer and dehydrated in ethanol (Huangfu et al., 2003). SEM was performed using a field emission microscope (Supra 25, Carl Zeiss), and images were acquired with SmartSEM (Carl Zeiss). For TEM, samples were postfixed with 1% osmium tetroxide followed by 1% uranyl acetate, dehydrated through a graded ethanol series and embedded in LX112 resin (Ladd Research Industries). Ultrathin sections were cut on an ultramicrotome (Reichert Ultracut, Leica), stained with uranyl acetate followed by lead citrate, and viewed on a transmission electron microscope (1200 EX, JEOL) at 5 kV.

Measurements of F-actin and G-actin

The G-actin/F-actin In Vivo Assay Kit (Cytoskeleton, BK037) was used according to the manufacturer's instructions. Pools of E9.5 WT and $Cfl1^{C5}$ embryos (three each), after manual removal of the heart, were lysed in 300 μl Lysis Buffer (LSA2). 100 μl lysate was used for the assay. Quantification of the bands was performed using the Gels tool from ImageJ.

Immunoblotting

A pool of heads of three E9.5 embryos, after removal of the heart, was lysed in Cell Lysis Buffer (Cytoskeleton, GL36) plus Complete Protease Inhibitor Cocktail (Roche). Western blots were performed according to standard protocols, and protein was detected with HRP-conjugated secondary antibodies and ECL detection reagents (Amersham). Immunoblots prepared from the same pools of control and mutant embryos were quantified using the Gels tool of ImageJ.

Acknowledgements

We thank Dr James R. Bamburg and Dr Masatoshi Takeichi for SHROOM3 antibodies; Dr Jennifer Zallen and members of K.V.A. laboratory for thoughtful comments on the manuscript; Vitaly Boiko for helping with 3D images; and the MSKCC Molecular Core Facility for valuable technical support. Monoclonal antibodies were obtained from the Developmental Studies Hybridoma Bank, created by the NICHD of the NIH and maintained at The University of Iowa, Department of Biology, Iowa City, IA 52242, USA.

Competing interests

The authors declare no competing or financial interests.

Author contributions

J.G.-B. planned and performed experiments and data analysis, prepared and edited the figures and wrote the manuscript. J.H. provided *Shroom3* mutant embryos. K.V.A. developed the concepts and approach and wrote the manuscript.

Funding

The work was supported by National Institute of Health grants [R37 HD03455 and R01 NS044385] to K.V.A.; the MSKCC Cancer Center Support Grant [P30 CA008748]; and a Beatriu de Pinós postdoctoral fellowship from Generalitat de Catalunya and an EMBO long-term fellowship to J.G.-B. Deposited in PMC for release after 12 months.

Supplementary material

Supplementary material available online at
http://dev.biologists.org/lookup/suppl/doi:10.1242/dev.115493/-/DC1

References

Bamburg, J. R., McGough, A. and Ono, S. (1999). Putting a new twist on actin: ADF/cofilins modulate actin dynamics. *Trends Cell Biol.* **9**, 364-370.

Baum, B. and Perrimon, N. (2001). Spatial control of the actin cytoskeleton in Drosophila epithelial cells. *Nat. Cell Biol.* **3**, 883-890.

Ben-Aissa, K., Patino-Lopez, G., Belkina, N. V., Maniti, O., Rosales, T., Hao, J.-J., Kruhlak, M. J., Knutson, J. R., Picart, C. and Shaw, S. (2012). Activation of moesin, a protein that links actin cytoskeleton to the plasma membrane, occurs by phosphatidylinositol 4,5-bisphosphate (PIP2) binding sequentially to two sites and releasing an autoinhibitory linker. *J. Biol. Chem.* **287**, 16311-16323.

Bernstein, B. W. and Bamburg, J. R. (2010). ADF/Cofilin: a functional node in cell biology. *Trends Cell Biol.* **20**, 187-195.

Blair, A. (2006). Twinstar, the Drosophila homolog of cofilin/ADF, is required for planar cell polarity patterning. *Development* **133**, 1789-1797.

Bloomekatz, J., Grego-Bessa, J., Migeotte, I. and Anderson, K. V. (2012). Pten regulates collective cell migration during specification of the anterior-posterior axis of the mouse embryo. *Dev. Biol.* **364**, 192-201.

Bravo-Cordero, J. J., Magalhaes, M. A. O., Eddy, R. J., Hodgson, L. and Condeelis, J. (2013). Functions of cofilin in cell locomotion and invasion. *Nat. Rev. Mol. Cell Biol.* **14**, 405-417.

Bresnick, A. R. (1999). Molecular mechanisms of nonmuscle myosin-II regulation. *Curr. Opin. Cell Biol.* **11**, 26-33.

Caspary, T., Larkins, C. E. and Anderson, K. V. (2007). The graded response to sonic hedgehog depends on cilia architecture. *Dev. Cell* **12**, 767-778.

Chen, X. and Macara, I. G. (2005). Par-3 controls tight junction assembly through the Rac exchange factor Tiam1. *Nat. Cell Biol.* **7**, 262-269.

Chen, X. and Macara, I. G. (2006). Par-3 mediates the inhibition of LIM kinase 2 to regulate cofilin phosphorylation and tight junction assembly. *J. Cell Biol.* **172**, 671-678.

Chen, Q. and Pollard, T. D. (2011). Actin filament severing by cofilin is more important for assembly than constriction of the cytokinetic contractile ring. *J. Cell Biol.* **195**, 485-498.
Colas, J.-F. and Schoenwolf, G. C. (2001). Towards a cellular and molecular understanding of neurulation. *Dev. Dyn.* **221**, 117-145.
Copp, A. J. and Greene, N. D. E. (2010). Genetics and development of neural tube defects. *J. Pathol.* **220**, 217-230.
del Barrio, M. G. and Nieto, M. A. (2002). Overexpression of Snail family members highlights their ability to promote chick neural crest formation. *Development* **129**, 1583-1593.
Ding, S.-J., Li, Y., Shao, X.-X., Zhou, H., Zeng, R., Tang, Z.-Y. and Xia, Q.-C. (2004). Proteome analysis of hepatocellular carcinoma cell strains, MHCC97-H and MHCC97-L, with different metastasis potentials. *Proteomics* **4**, 982-994.
Eom, D. S., Amarnath, S. and Agarwala, S. (2013). Apicobasal polarity and neural tube closure. *Dev. Growth Differ.* **55**, 164-172.
Fanning, A. S., Jameson, B. J., Jesaitis, L. A. and Anderson, J. M. (1998). The tight junction protein ZO-1 establishes a link between the transmembrane protein occludin and the actin cytoskeleton. *J. Biol. Chem.* **273**, 29745-29753.
García-García, M. J., Eggenschwiler, J. T., Caspary, T., Alcorn, H. L., Wyler, M. R., Huangfu, D., Rakeman, A. S., Lee, J. D., Feinberg, E. H., Timmer, J. R. et al. (2005). Analysis of mouse embryonic patterning and morphogenesis by forward genetics. *Proc. Natl. Acad. Sci. USA* **102**, 5913-5919.
Gunsalus, K. C., Bonaccorsi, S., Williams, E., Verni, F., Gatti, M. and Goldberg, M. L. (1995). Mutations in twinstar, a Drosophila gene encoding a cofilin/ADF homologue, result in defects in centrosome migration and cytokinesis. *J. Cell Biol.* **131**, 1243-1259.
Gurniak, C. B., Perlas, E. and Witke, W. (2005). The actin depolymerizing factor n-cofilin is essential for neural tube morphogenesis and neural crest cell migration. *Dev. Biol.* **278**, 231-241.
Hadjantonakis, A.-K., Cox, L. L., Tam, P. P. L and Nagy, A. (2001). An X-linked GFP transgene reveals unexpected paternal X-chromosome activity in trophoblastic giant cells of the mouse placenta. *Genesis* **29**, 133-140.
Hildebrand, J. D. (2005). Shroom regulates epithelial cell shape via the apical positioning of an actomyos in network. *J. Cell Sci.* **118**, 5191-5203.
Hildebrand, J. D. and Soriano, P. (1999). Shroom, a PDZ domain-containing actin-binding protein, is required for neural tube morphogenesis in mice. *Cell* **99**, 485-497.
Huangfu, D., Liu, A., Rakeman, A. S., Murcia, N. S., Niswander, L. and Anderson, K. V. (2003). Hedgehog signalling in the mouse requires intraflagellar transport proteins. *Nature* **426**, 83-87.
Ivanov, A. I. (2008). Actin motors that drive formation and disassembly of epithelial apical junctions. *Front. Biosci.* **13**, 6662-6681.
Ivanov, A. I., McCall, I. C., Parkos, C. A. and Nusrat, A. (2004). Role for actin filament turnover and a myosin II motor in cytoskeleton-driven disassembly of the epithelial apical junctional complex. *Mol. Biol. Cell* **15**, 2639-2651.
Ivanov, A. I., Hunt, D., Utech, M., Nusrat, A. and Parkos, C. A. (2005). Differential roles for actin polymerization and a myosin II motor in assembly of the epithelial apical junctional complex. *Mol. Biol. Cell* **16**, 2636-2650.
Koleske, A. J., Gifford, A. M., Scott, M. L., Nee, M., Bronson, R. T., Miczek, K. A. and Baltimore, D. (1998). Essential roles for the Abl and Arg tyrosine kinases in neurulation. *Neuron* **21**, 1259-1272.
Lanier, L. M., Gates, M. A., Witke, W., Menzies, A. S., Wehman, A. M., Macklis, J. D., Kwiatkowski, D., Soriano, P. and Gertler, F. B. (1999). Mena is required for neurulation and commissure formation. *Neuron* **22**, 313-325.
Lee, H.-Y., Kosciuk, M. C., Nagele, R. G. and Roisen, F. J. (1983). Studies on the mechanisms of neurulation in the chick: possible involvement of myosin in elevation of neural folds. *J. Exp. Zool.* **225**, 449-457.
Lee, J. D., Silva-Gagliardi, N. F., Tepass, U., McGlade, C. J. and Anderson, K. V. (2007). The FERM protein Epb4.1l5 is required for organization of the neural plate and for the epithelial-mesenchymal transition at the primitive streak of the mouse embryo. *Development* **134**, 2007-2016.
Lee, J. D., Migeotte, I. and Anderson, K. V. (2010). Left-right patterning in the mouse requires Epb4.1l5-dependent morphogenesis of the node and midline. *Dev. Biol.* **346**, 237-246.
Mahaffey, J. P., Grego-Bessa, J., Liem, K. F. and Anderson, K. V. (2013). Cofilin and Vangl2 cooperate in the initiation of planar cell polarity in the mouse embryo. *Development* **140**, 1262-1271.
McCaffrey, L. M. and Macara, I. G. (2011). Epithelial organization, cell polarity and tumorigenesis. *Trends Cell Biol.* **21**, 727-735.
Mendes Pinto, I., Rubinstein, B., Kucharavy, A., Unruh, J. R. and Li, R. (2012). Actin depolymerization drives actomyosin ring contraction during budding yeast cytokinesis. *Dev. Cell* **22**, 1247-1260.
Meng, Y., Takahashi, H., Meng, J., Zhang, Y., Lu, G., Asrar, S., Nakamura, T. and Jia, Z. (2004). Regulation of ADF/cofilin phosphorylation and synaptic function by LIM-kinase. *Neuropharmacology* **47**, 746-754.
Menzies, A. S., Aszodi, A., Williams, S. E., Pfeifer, A., Wehman, A. M., Goh, K. L., Mason, C. A., Fassler, R. and Gertler, F. B. (2004). Mena and vasodilator-stimulated phosphoprotein are required for multiple actin-dependent processes that shape the vertebrate nervous system. *J. Neurosci.* **24**, 8029-8038.
Mitchell, L. E. (2005). Epidemiology of neural tube defects. *Am. J. Med. Genet.* **135C**, 88-94.
Nishimura, T. and Takeichi, M. (2008). Shroom3-mediated recruitment of Rho kinases to the apical cell junctions regulates epithelial and neuroepithelial planar remodeling. *Development* **135**, 1493-1502.
Norden, C., Young, S., Link, B. A. and Harris, W. A. (2009). Actomyosin is the main driver of interkinetic nuclear migration in the retina. *Cell* **138**, 1195-1208.
Ono, K., Parast, M., Alberico, C., Benian, G. M. and Ono, S. (2003). Specific requirement for two ADF/cofilin isoforms in distinct actin-dependent processes in Caenorhabditis elegans. *J. Cell Sci.* **116**, 2073-2085.
Pelham, R. J. and Chang, F. (2002). Actin dynamics in the contractile ring during cytokinesis in fission yeast. *Nature* **419**, 82-86.
Pham, H., Yu, H. and Laski, F. A. (2008). Cofilin/ADF is required for retinal elongation and morphogenesis of the Drosophila rhabdomere. *Dev. Biol.* **318**, 82-91.
Roignot, J., Peng, X. and Mostov, K. (2013). Polarity in mammalian epithelial morphogenesis. *Cold Spring Harb. Perspect. Biol.* **5**, a013789.
Schoenwolf, G. C. (1985). Shaping and bending of the avian neuroepithelium: morphometric analyses. *Dev. Biol.* **109**, 127-139.
Sinha, P., Hütter, G., Köttgen, E., Dietel, M., Schadendorf, D. and Lage, H. (1999). Increased expression of epidermal fatty acid binding protein, cofilin, and 14-3-3-σ (stratifin) detected by two-dimensional gel electrophoresis, mass spectrometry and microsequencing of drug-resistant human adenocarcinoma of the pancreas. *Electrophoresis* **20**, 2952-2960.
Smith-Beckerman, D. M., Fung, K. W., Williams, K. E., Auersperg, N., Godwin, A. K. and Burlingame, A. L. (2005). Proteome changes in ovarian epithelial cells derived from women with BRCA1 mutations and family histories of cancer. *Mol. Cell. Proteomics* **4**, 156-168.
Spear, P. C. and Erickson, C. A. (2012). Interkinetic nuclear migration: a mysterious process in search of a function. *Dev. Growth Differ.* **54**, 306-316.
Tepass, U. (2012). The apical polarity protein network in drosophila epithelial cells: regulation of polarity, junctions, morphogenesis, cell growth, and survival. *Annu. Rev. Cell Dev. Biol.* **28**, 655-685.
Thiery, J. P., Acloque, H., Huang, R. Y. J. and Nieto, M. A. (2009). Epithelial-mesenchymal transitions in development and disease. *Cell* **139**, 871-890.
Tsukita, S., Oishi, K., Sato, N., Sagara, J., Kawai, A. and Tsukita, S. (1994). ERM family members as molecular linkers between the cell surface glycoprotein CD44 and actin-based cytoskeletons. *J. Cell Biol.* **126**, 391-401.
Unwin, R. D., Craven, R. A., Harnden, P., Hanrahan, S., Totty, N., Knowles, M., Eardley, I., Selby, P. J. and Banks, R. E. (2009). Proteomic changes in renal cancer and co-ordinate demonstration of both the glycolytic and mitochondrial aspects of the Warburg effect. *Proteomics* **3**, 1620-1632.
Wang, W., Mouneimne, G., Sidani, M., Wyckoff, J., Chen, X., Makris, A., Goswami, S., Bresnick, A. R. and Condeelis, J. S. (2006). The activity status of cofilin is directly related to invasion, intravasation, and metastasis of mammary tumors. *J. Cell Biol.* **173**, 395-404.
Wang, W., Eddy, R. and Condeelis, J. (2007). The cofilin pathway in breast cancer invasion and metastasis. *Nat. Rev. Cancer* **7**, 429-440.
Wiggan, O., Shaw, A. E., DeLuca, J. G. and Bamburg, J. R. (2012). ADF/cofilin regulates actomyosin assembly through competitive inhibition of myosin II binding to F-actin. *Dev. Cell* **22**, 530-543.
Zhang, L., Luo, J., Wan, P., Wu, J., Laski, F. and Chen, J. (2011). Regulation of cofilin phosphorylation and asymmetry in collective cell migration during morphogenesis. *Development* **138**, 455-464.
Zhu, H., Enaw, J. O. E., Ma, C., Shaw, G. M., Lammer, E. J. and Finnell, R. H. (2007). Association between CFL1 gene polymorphisms and spina bifida risk in a California population. *BMC Med. Genet.* **8**, 12.
Zumdieck, A., Kruse, K., Bringmann, H., Hyman, A. A. and Jülicher, F. (2007). Stress generation and filament turnover during actin ring constriction. *PLoS ONE* **2**, e696.

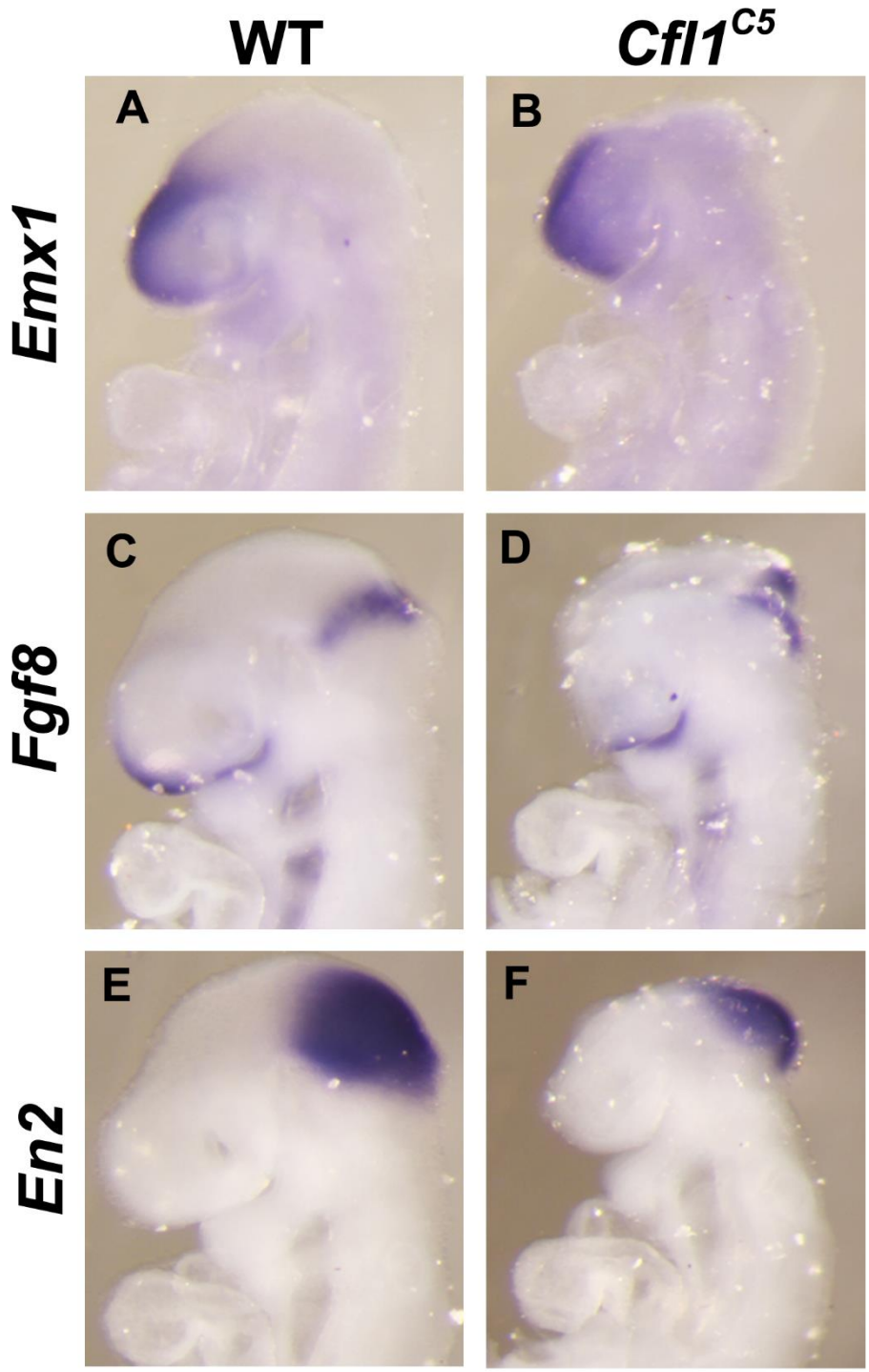

Figure S1. Normal anterior-posterior patterning in the developing *Cfl1*^{C5} brain.
In situ hybridization of E9.5 WT and *Cfl1*^{C5} embryos with **A, B)** the forebrain marker *emx1*, **C, D)** the midbrain-hindbrain junction marker *fgf8* and **E, F)** the hindbrain marker *en2*.

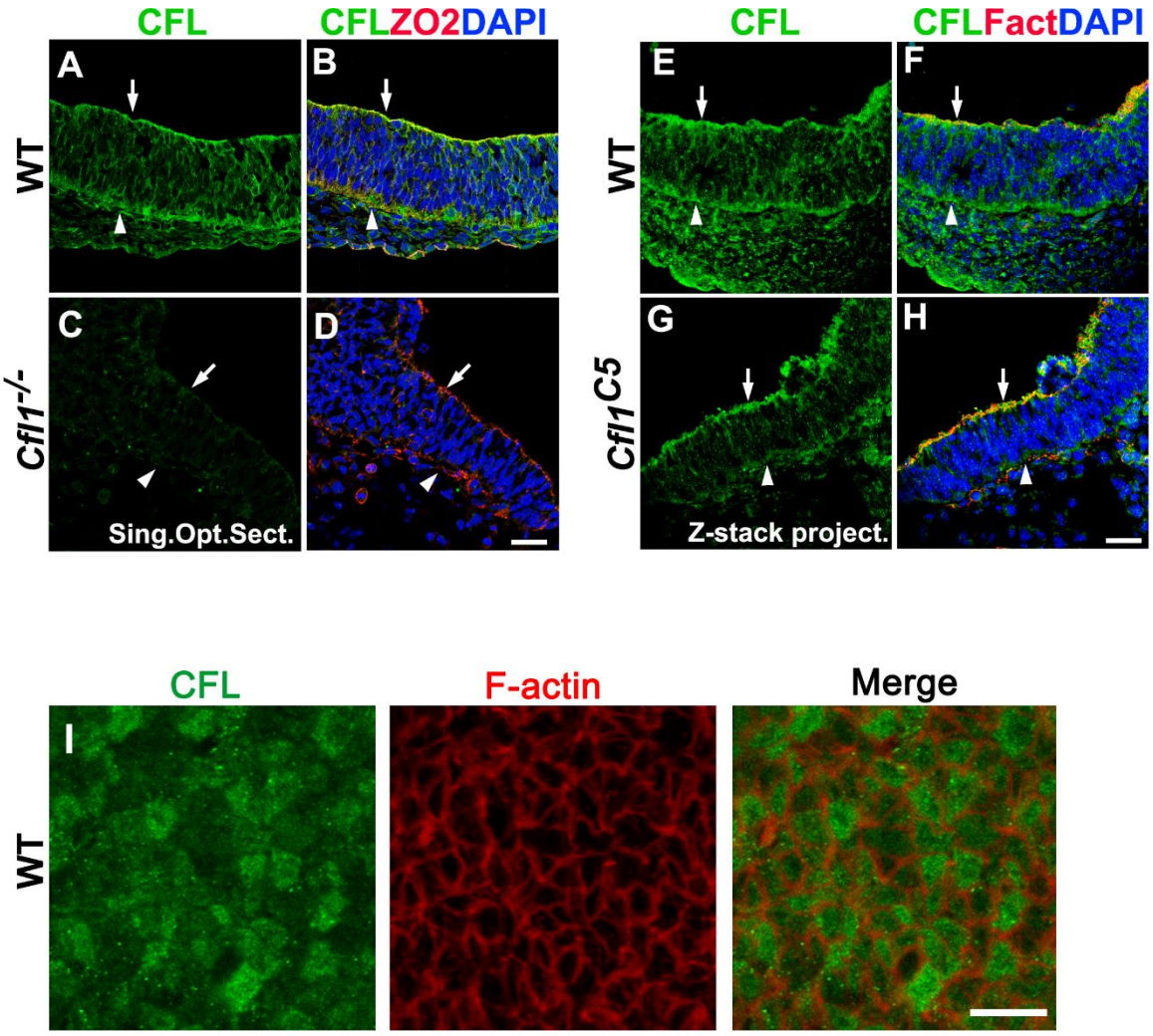

Figure S2. CFL expression in WT and *Cfl1*^{tm1Wit} E9.5 neural plate.
Immunodetection of CFL and ZO2 in transverse sections of WT (**A, B**) and the *Cfl1*^{tm1Wit} **null** allele at E9.5 (**C, D**) shows the specificity of CFL staining. Z-stack projection of 3 optical sections taken every 1μm, showing double staining of CFL and F-actin in WT (**E, F**) and *Cfl1*^{C5} (**G, H**) transverse sections. **(I)** *en face* images of CFL (green) and F-actin (red) expression of the apical domain of wild-type E9.5 cephalic neural tube. Arrows indicate apical, arrowheads indicate basal. Scale bar in A-D is 30 μm; in E is 10 μm.

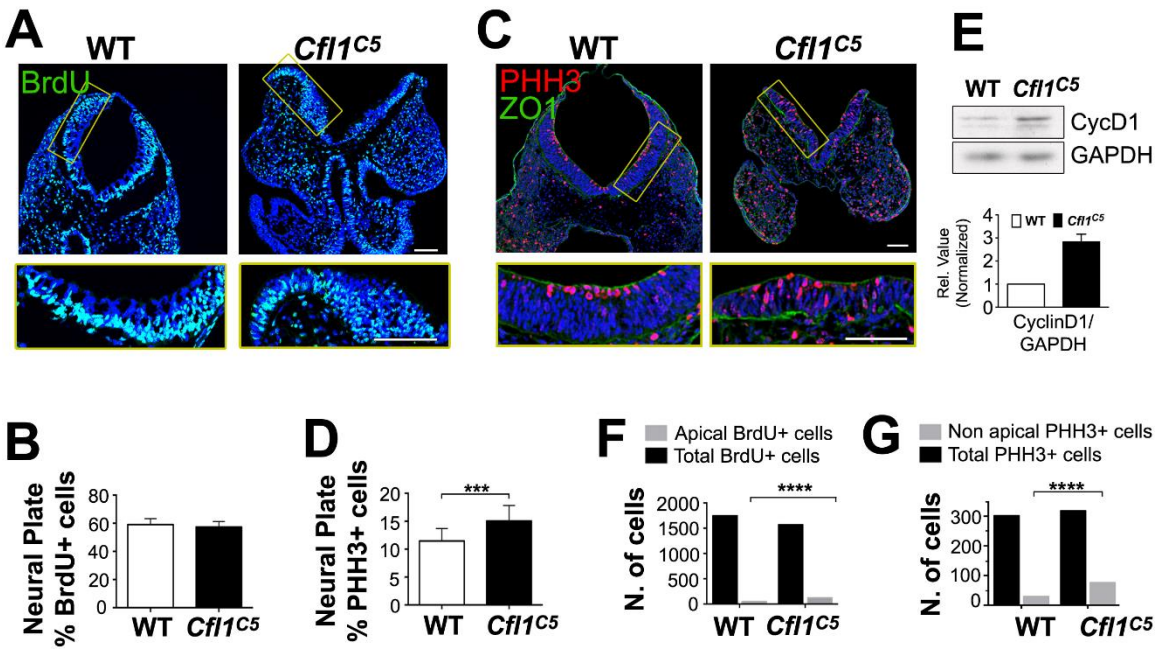

Figure S3. Proliferation analysis in *Cfl1*^{C5} mutant embryos.

A) BrdU^{+} cells (green) after a 25 min pulse in E9.5 WT and *Cfl1*^{C5} transverse cephalic sections. **B)** Quantification S-phase neural plate cells. WT: 1692 BrdU^{+} cells out of 3024 total, n=3 embryos; 56 ± 5%. *Cfl1*^{C5}: 1578 BrdU^{+} cells out of 2871 cells, n=3 embryos; 55 ± 4%; p = 0.0932; **C)** Phospho-histone H3 (PHH3) (red) and ZO1 (green) staining in E9.5 WT and *Cfl1*^{C5} transverse cephalic sections. **D)** Mitotic index of cephalic neural plate: WT: 277 PHH3^{+} cells out of 2321 total; 12 ± 2%; *Cfl1*^{C5}: 224 PHH3^{+} cells out of 1361; 15 ± 3%; ***p = 0.0001. **E**) Western blot of Cyclin D1 and GAPDH, and quantification normalized to WT. **F-G)** Analysis of interkinetic nuclear migration. **F**) Quantification of apical BrdU^{+} cells. WT: 48 apical BrdU^{+} out of 1747 cells, n=3 embryos; 3 ± 1%. *Cfl1*^{C5}: 123 apical BrdU^{+} out of 1569 cells, n=3 embryos; 8 ± 2%; ****p < 0.0001. **G)** Quantification of non-apical mitotic cells: WT: 29 out of 302; 10 ± 2%; *Cfl1*^{C5}: 76 out of 318; 24 ± 11%; ****p < 0.0001. Scale bars: A and D 80 μm. Statistical analysis was performed using Chi square (Fisher's exact) test. Error bars indicate standard deviation.

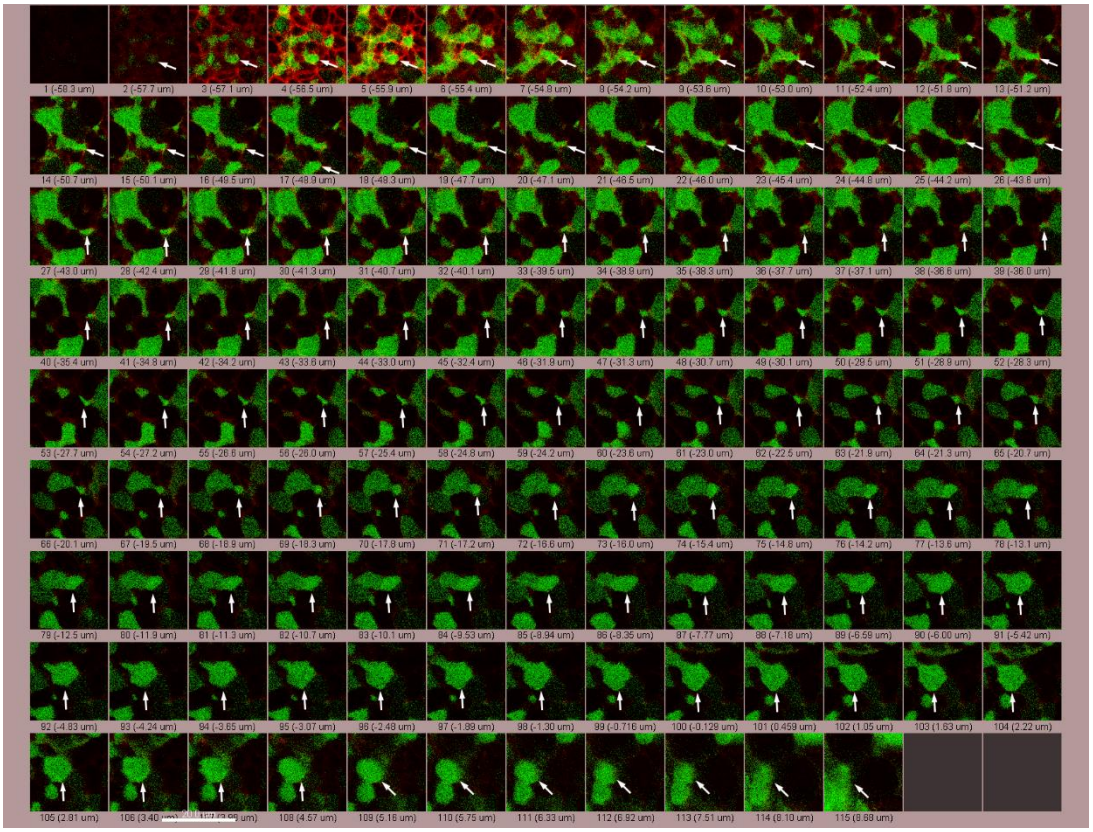

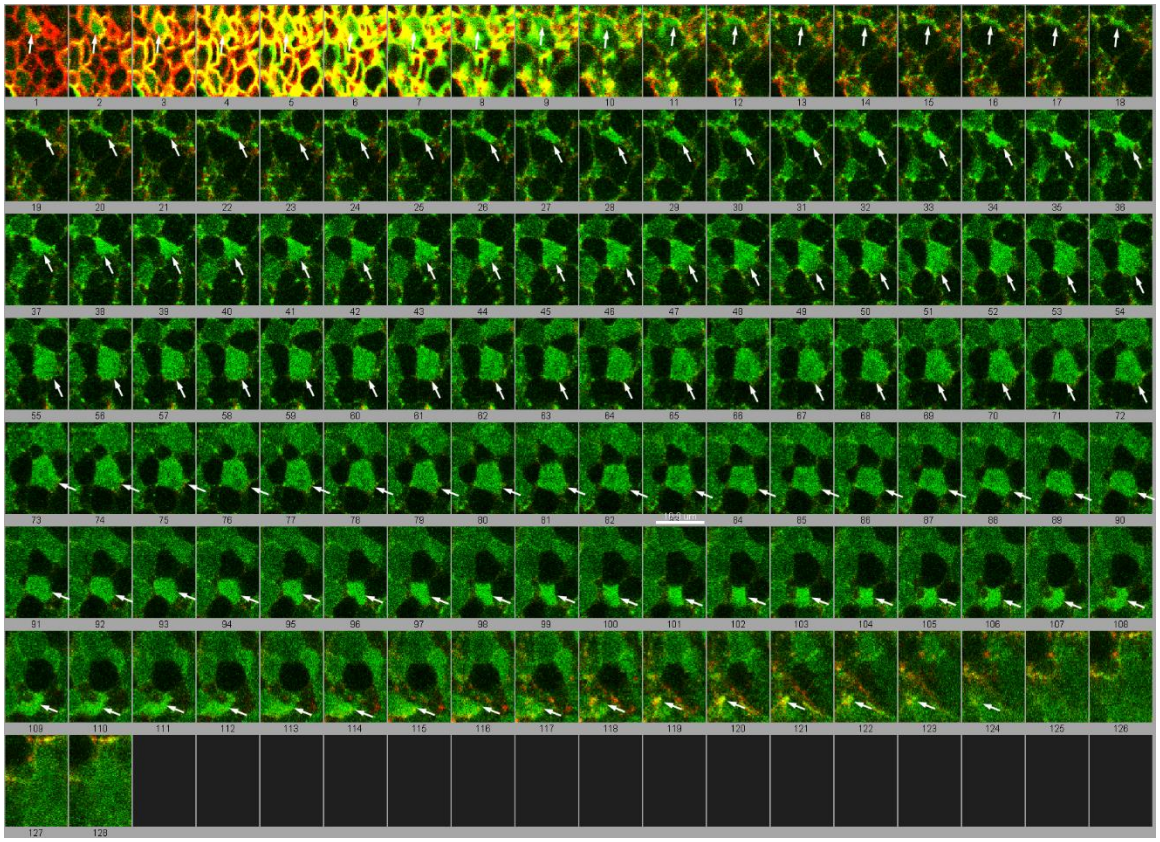

Figure S4 and S5. Single optical sections along the Z axis of WT (Fig. S4) and *Cfl1*^{C5} (Fig. S5) neuroepithelium.

Single planes used to make the 3D rendering shown in Fig. 3D. Red is F-actin: Green is X-linked GFP. Arrows point a single cell along the apicobasal axis.

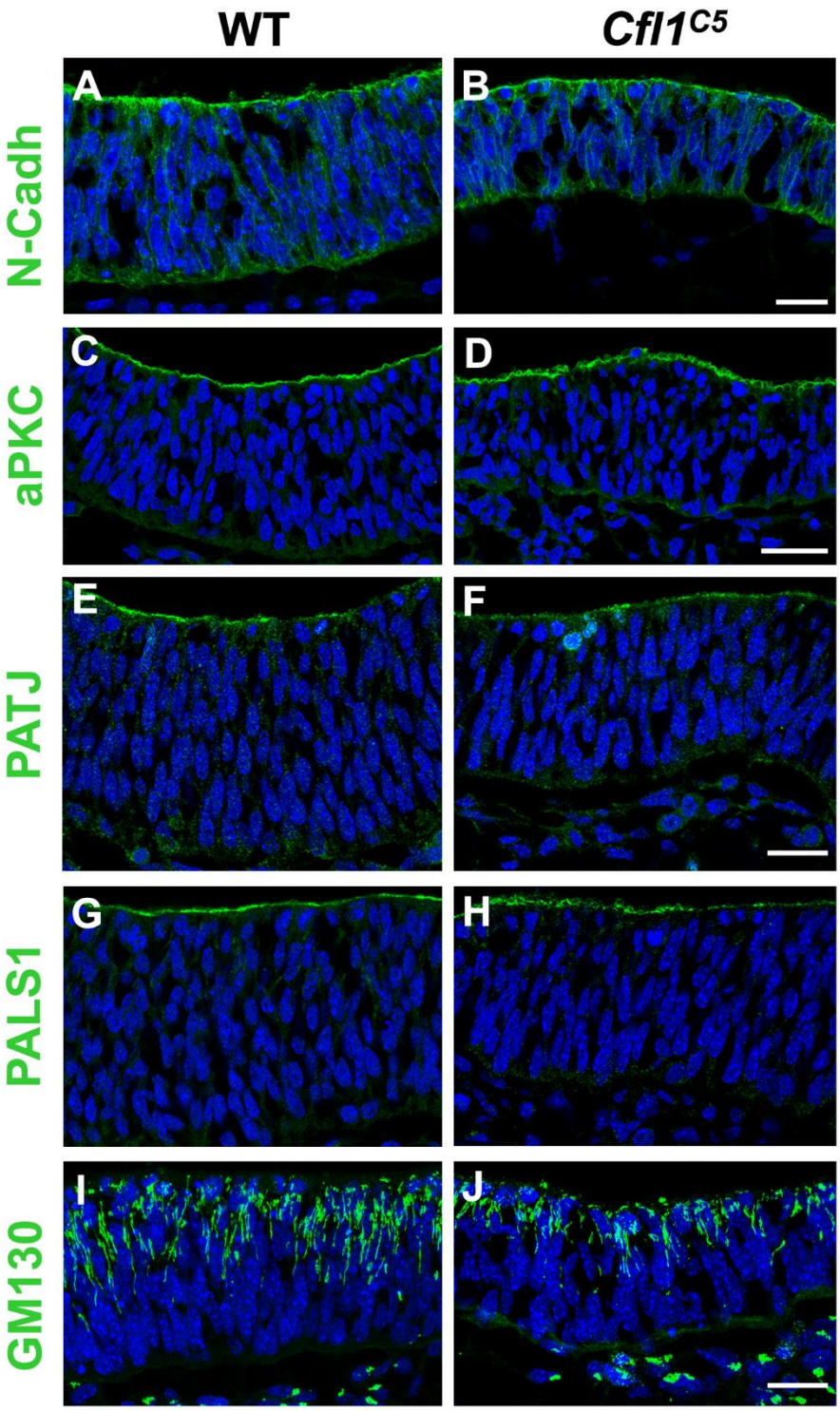

Figure S6. Normal apical-basal polarity marker expression in the *Cfl1*^{C5} neural plate. Transverse sections of E9.5 WT and *Cfl1*^{C5} cephalic neural plates stained for **A, B)** N-Cadherin, **C, D)** aPKC, **E, F)** PATJ, **G, H)** PALS1, **I, J)** GM130. Blue is DAPI. **A**, **B**, **I** and **J** are Z-stack projections of 3 single optical sections taken every 1μm. Scale bar is 30μm.

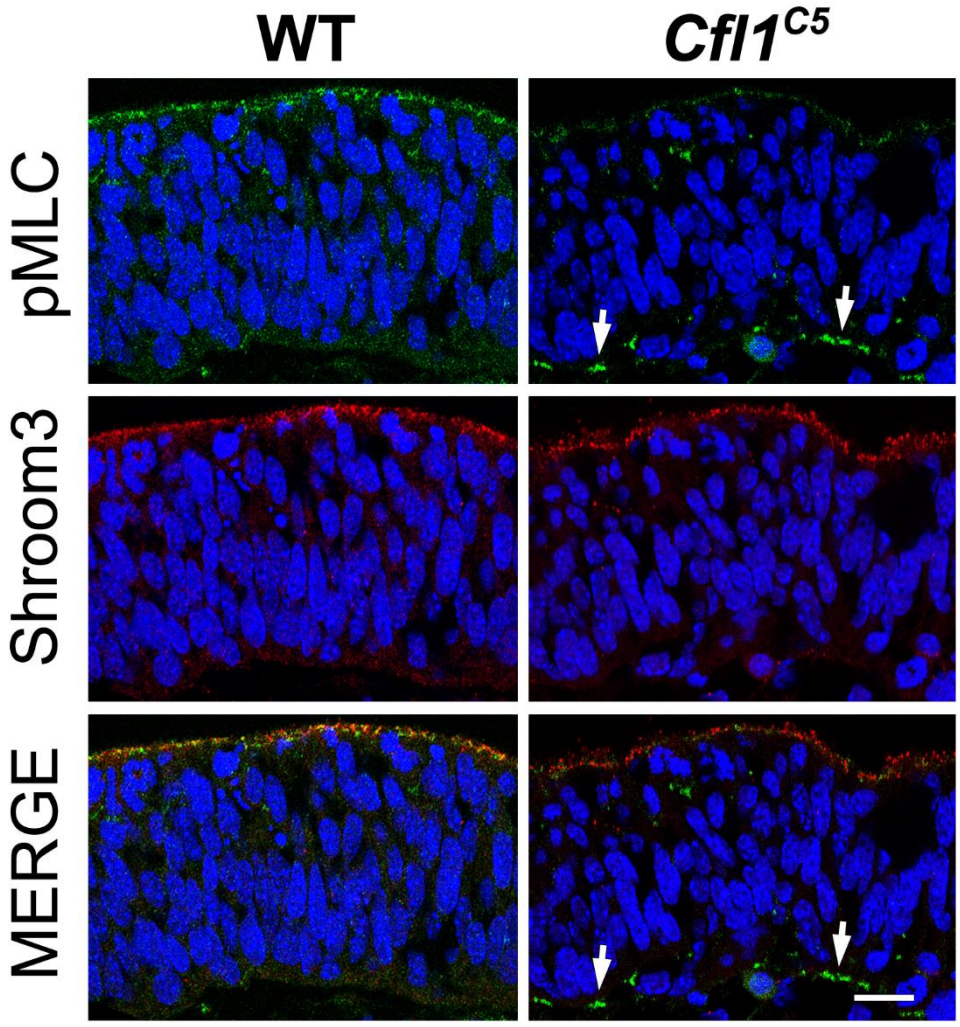

Figure S7. Double labeling of pMLC and SHROOM3 in WT and *Cfl1*^{C5}embryos at E9.5.

Z-stack projections of 3 optical sections taken every 1 μm. from a cephalic transverse section. Arrows indicates ectopic localization. Scale bar is 30 μm.

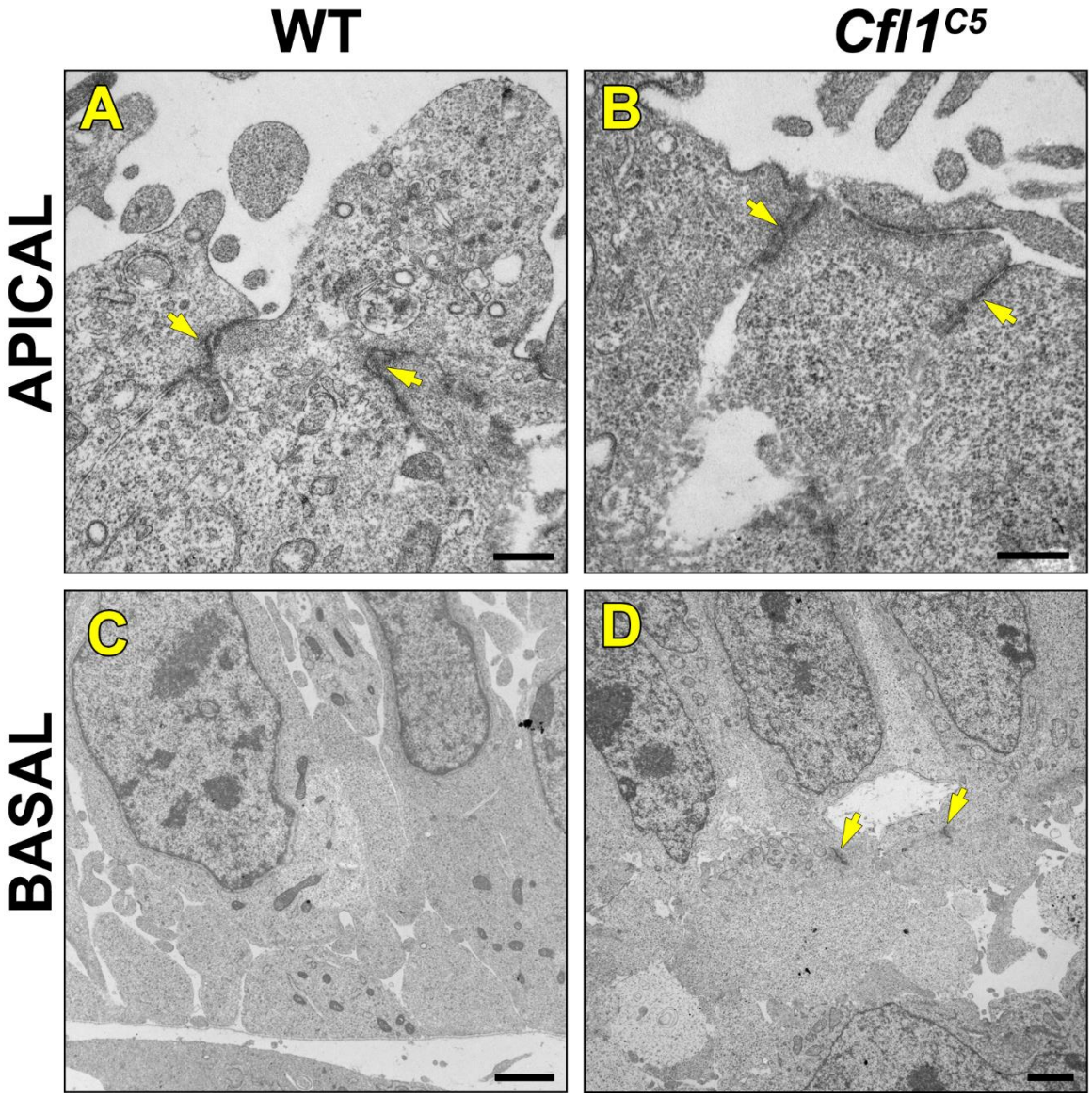

Figure S8. Ultrastructure of apical and basal domains of cephalic neural plate.
TEM analysis of E9.5 WT and *Cfl1*^{C5} cephalic neural plates. **A, B)** Apical domain: **B, C)** Basal domain. Arrows indicate electron-dense particles. Scale bar in A and B is 500nm; in C and D is 2μm.

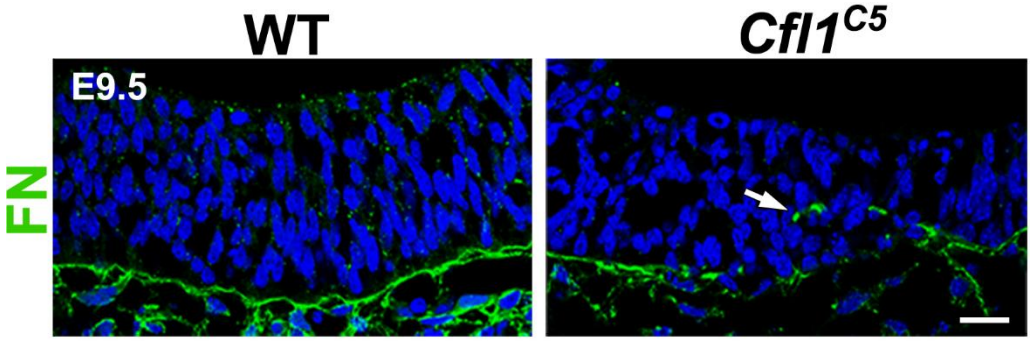

Figure S9. Ectopic localization of fibronectin in *Cfl1*^{C5} and ectopic cell clusters in the *Cfl1*^{C5} neural plate A) Fibronectin expression in E9.5 cephalic neural plate. Arrows indicate ectopic expression. Blue is DAPI. Scale bar 30 μm.

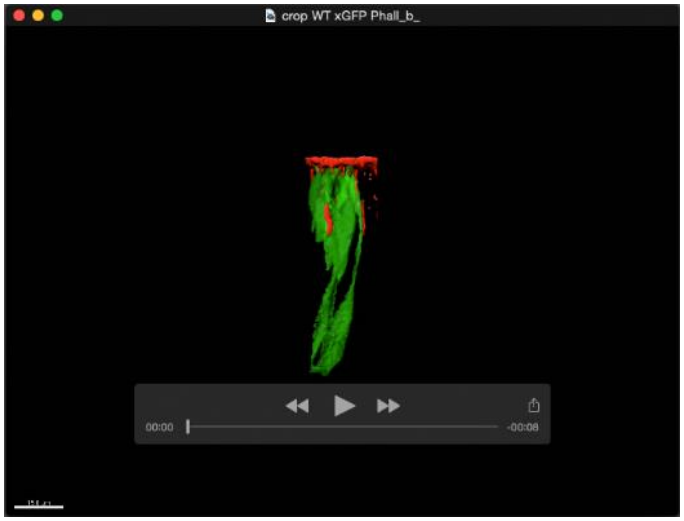

Movie 1. 3D rendering of a E9.5 WT X-linked GFP^{+} cephalic neuroepithelial cell. F-actin (red) is apical; no overlapping signal can be detected at the basal domain.

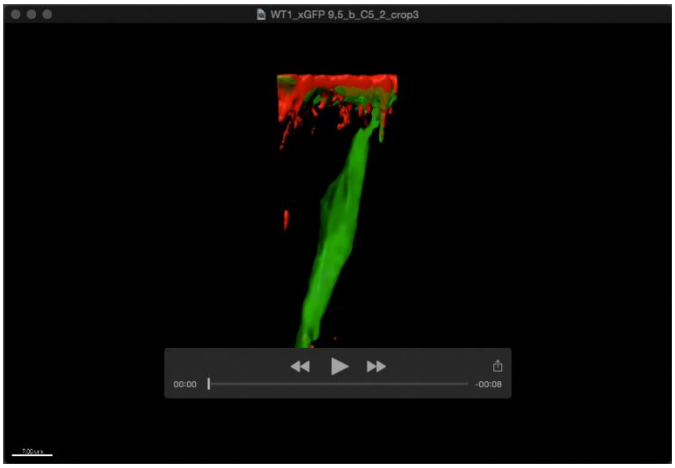

Movie 2. 3D rendering of a E9.5 *Cfl1*^{C5} X-linked GFP^{+} cephalic neuroepithelial cell. F-actin (red) is apical and basal, overlapping with endogenous GFP.